Check for updates

ChemistryEurope

ChemistryEurope
Excellence in Chemistry Research Worldwide

RESEARCH ARTICLE OPEN ACCESS

Nickel(0)-Catalyzed [2+2+2] Cycloadditions of Linked Bisdiynes with Diaryl Alkynes Generates D-π-A-π-D Bis(arylethynyl)indane-Based Organic Frameworks as Noncytotoxic Probes for Ds-DNA/Ds-RNA

Robert Ricker[1] | Dijana Pavlović Saftić[2] | Sabine Lorenzen[1] | Johannes Schneider[1] | Alena Neudert[1] | Michelle Kalizki[1] | Johannes Krebs[1] | Florian Kerner[1] | Alexandra Friedrich[1] | Ludwig Zapf[1] | Nils Schopper[1] | Maik Finze[1] | Nina Vukadinović[2] | Lucija Lulić Horvat[3] | Ivo Piantanida[2] | Todd B. Marder[1]

[1]Institut für Anorganische Chemie, and Institute for Sustainable Chemistry & Catalysis with Boron, Julius-Maximilians-Universität Würzburg, Würzburg, Germany | [2]Division of Organic Chemistry & Biochemistry, Ruđer Bošković Institute, Zagreb, Croatia | [3]Division of Molecular Biology, Ruđer Bošković Institute, Zagreb, Croatia

Correspondence: Ivo Piantanida (pianta@irb.hr) | Todd B. Marder (todd.marder@uni-wuerzburg.de)

Received: 19 November 2025 | **Revised:** 7 March 2026 | **Accepted:** 12 March 2026

Keywords: [2+2+2] cycloaddition | biomolecule sensing | DNA | fluorescence | nickel | RNA

ABSTRACT

Nickel(0)-catalyzed [2 + 2 + 2] cycloadditions of linked bisdiynes with diarylacetylenes were performed using the Ni(II) precursor complex [(TMEDA)Ni(*o*-tolyl)Cl] in the presence of PPh_3 ligands to generate the active Ni(0) species. Optimal reactivity was observed when electron-rich bisdiynes reacted with electron-deficient diarylacetylenes, affording air-stable, approximately C_{2v}-symmetric D-π-A-π-D bis(arylethynyl)indane-based dyes containing *o*-terphenyl cores. Spectroscopic analyses revealed strong solvatochromic emission with high quantum yields in solution, except for the nonemissive bis-*N*-methylpyridinium derivative 4,4′-(4,7-bis((4-(bis(4-methoxyphenyl)amino)phenyl)ethynyl)−2,3-dihydro-1H-indene-5,6-diyl)bis(1-methylpyridin-1-ium) ditriflate, **10**, pointing toward the decisive impact of pyridine methylation on the nonradiative relaxation of the fluorophore. Vibrational studies of the triarylamine dyes displayed a prominent alkyne stretching band in both Raman and IR spectra, applicable for use as a probe. Biorelevant studies revealed that the synthesized dyes bind strongly to double-stranded DNA and RNA, most likely through groove insertion, leading to significant fluorescence quenching. Only the dicationic derivative **10** showed a characteristic CD response, attributed to additional electrostatic interactions that orient the dye within the DNA minor or RNA major groove. The dyes had minimal effects on polynucleotide thermal stability, suggesting that hydrophobic and van der Waals forces dominate the binding, except for derivative **10**, which also involves electrostatic interactions. All compounds were found to be nontoxic toward human cell lines, indicating their promise as multimodal fluorescence, CD, and Raman probes for intracellular and extracellular bioimaging applications.

1 | Introduction

Alkynylated aromatics can be used as materials for nonlinear optics, as fluorescent dyes, and in optoelectronic devices; examples of this include phenylene–ethynylene oligomers [1–3], such as bis(phenylethynyl)-benzenes [4, 5], -naphthalenes [6], and -anthracenes [3, 6–10]. The incorporation of alkyne units into arene-containing conjugated systems provides good electronic communication along with structural rigidity and stability [9, 11].

Robert Ricker and Dijana Pavlović Saftić contributed equally to this work.

This is an open access article under the terms of the Creative Commons Attribution License, which permits use, distribution and reproduction in any medium, provided the original work is properly cited.

© 2026 The Author(s). *ChemistryEurope* published by Chemistry Europe and Wiley-VCH GmbH.

Recently, we showed that conjugated triarylborane fluorophores are highly promising multifunctional probes for biomolecular recognition and imaging [12–18]. Quadrupolar bis(triarylboranes) incorporating diyne-, tetrayne-, or bis(arylethynyl)arenes in the bridge [19–22] can integrate strong fluorescence, high two-photon absorption cross-sections, Raman activity, high-affinity nucleic acid/protein binding, and light-triggered cytotoxicity. Their unusual biomolecule binding modes and tunable singlet oxygen sensitization establish them as promising candidates for theranostic applications [13, 20–22].

In other work, we have prepared various bis(arylethynyl)arenes, typically via Sonogashira cross-coupling reactions, and examined their linear and nonlinear optical properties and applications in biology [4, 7, 9, 11, 23]. In addition, we have reported the formation of bis(arylethynyl)rhodacyclopentadienes via coupling of two diynes, including linked bisdiynes, and studied their optical properties in detail [24–30]. Interestingly, those compounds are fluorescent [24], as is an iridium analog [28], even though a heavy transition metal is present. We [31, 32], and others [33–35], have also explored the metal-free cyclization of bisdiynes, now known as the hexa-dehydro Diels–Alder reaction, which can generate very interesting highly conjugated organic π-systems *via* benzyne intermediates.

On the other hand, metal-catalyzed [2 + 2 + 2] cycloaddition reactions of three alkynes, or two alkynes and a nitrile, are a convenient tool to construct complex organic molecules [36–47]. In materials chemistry, cyclization reactions of unsaturated precursors represent one of the best ways to create carbon-rich scaffolds [23]. The most common metals used for [2 + 2 + 2] cyclizations are Co and Rh, although Ni-catalysts are becoming more widely used [48]. A common synthetic strategy is to tether two or more of the alkyne units to achieve a higher degree of selectivity [49–52]. However, there is not much to be found in the literature regarding metal-catalyzed linked bisdiyne cyclizations [53]. In previous work, our group found that [Rh(κ^2-*S*,*S*'-S_2CNEt_2)(PPh_3)$_2$] catalyzes the formation of dimers and trimers of bisdiynes in varying ratios, depending on the substituents on the bisdiyne and the amount of catalyst used [54] (Figure 1).

Combining our various interests with all of the above information, we decided to explore the potential of a Ni-catalyst for the cyclo-co-trimerization of donor-substituted linked-bisdiynes with bis-acceptor-substituted alkynes to synthesize a series of highly luminescent D-π-A-π-D bis(arylethynyl)indanes (Scheme 1) and examine their cytotoxicity and binding to various DNA's and RNA's. The polynucleotides we employed to investigate the modes of binding were the most commonly used ds-DNA representatives with specific structural features (Supporting Information, Table S4): *calf thymus* (ct)-DNA characterized by a typical B-helical structure and approximately equimolar number of G-C and A-T base pairs; synthetic polynucleotides poly(dAdT)$_2$, and poly(dGdC)$_2$ also having a B-helical structure, but the latter one characterized by guanine amino groups sterically blocking the minor groove; and a synthetic ds-RNA representative: poly A–poly U, characterized by an A-helical structure [55, 56]. We also screened human cell viability (cytotoxicity) using the MTT test.

2 | Results and Discussion

2.1 | Synthesis

Initially, we explored the cyclization of bisdiyne **1a** with Ni(0) as the active metal catalyst, formed from the Ni(II) catalyst precursor [(TMEDA)Ni(*o*-tolyl)Cl] [57, 58], which gave the [2 + 2 + 2] product **2**, when the reaction was carried out in toluene at 100°C (Figure 2). The same product was previously formed when using a rhodium(I) catalyst, *vide supra*, and was fully characterized in that study [54]. The reaction did not show any conversion when run at temperatures below 60°C. In addition to the main product, trimers of **1a** were also detected in the reaction mixture *via* mass spectrometry but were not characterized further.

Then, the reaction was carried out in the presence of bis(4-cyanophenyl)acetylene **3** to see whether the dimerization of the bisdiyne **1a** would still be the prominent reaction or whether a co-cyclization product would be observed. Indeed, now, a [2 + 2 + 2] cyclization between the two substrates took place to form the bis(arylethynyl)indane derivative **4**, while **2** was only detected in trace amounts in the reaction mixture (Figure 3).

To elucidate the effects of different substitution patterns, a donor-containing *N*,*N*-dimethylaniline-substituted bisdiyne (**1b**) was combined with acetylenes bearing benzonitrile, methyl benzoate, or pyridine acceptor moieties, to obtain the bis(arylethynyl)

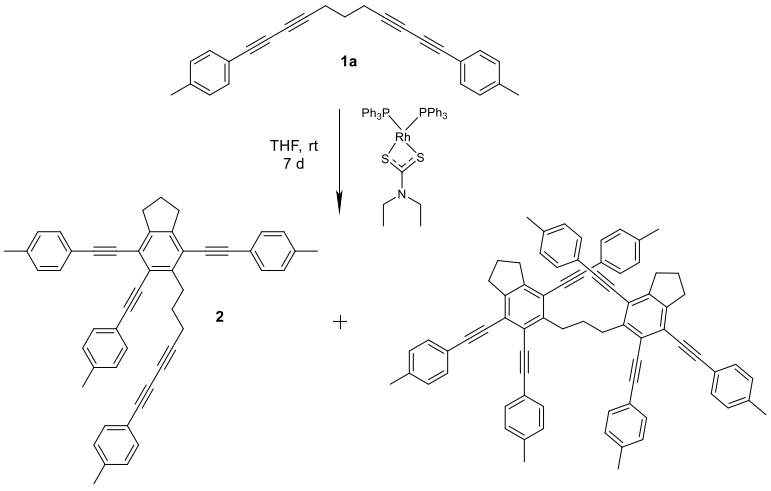

FIGURE 1 | Example of the Rh-catalyzed cyclodimerization and trimerization products from a linked bisdiyne previously isolated by our group [54].

27514765, 2026, 4, Downloaded from https://chemistry-europe.onlinelibrary.wiley.com/doi/10.1002/ceur.202500464 by Cochrane Croatia, Wiley Online Library on [24/11/2026]. See the Terms and Conditions (https://onlinelibrary.wiley.com/terms-and-conditions) on Wiley Online Library for rules of use; OA articles are governed by the applicable Creative Commons License

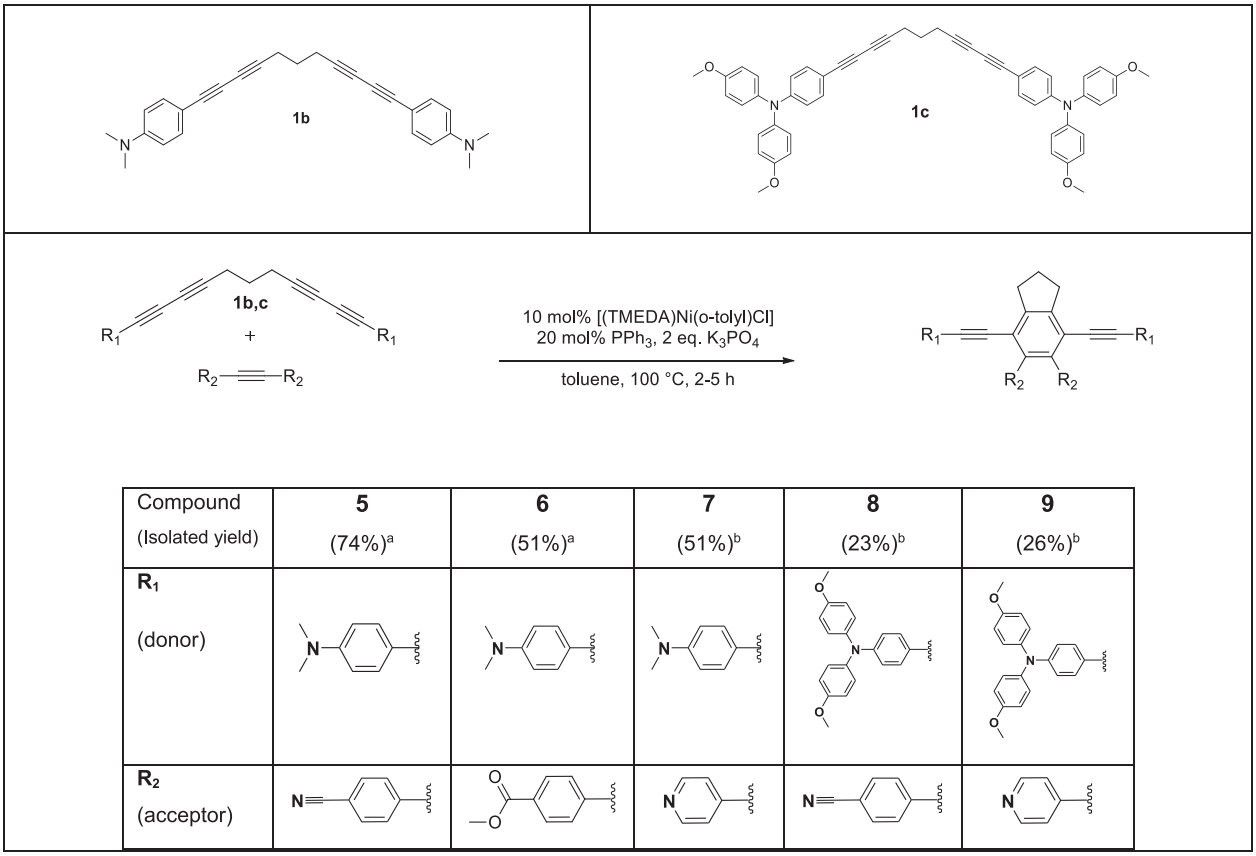

Compound (Isolated yield)	5 (74%)[a]	6 (51%)[a]	7 (51%)[b]	8 (23%)[b]	9 (26%)[b]
R_1 (donor)					
R_2 (acceptor)					

SCHEME 1 | Nickel-catalyzed bisdiyne-diphenylacetylene cyclization reactions. (a) Reaction carried out at 100°C for 5 h in an oil bath; (b) Reaction carried out at 100°C for 2 h in a microwave reactor; Upon heating to 100°C for 5 h in an oil bath for $R_1 = CN$, $R_2 = 4\text{-}CNPh$, the product was formed in < 10% yield and not examined further. For $R_1 = NMe_2$, $R_2 = 4\text{-}Me_2NPh$, the product was not observed, and for $R_1 = CN$, $R_2 = 4\text{-}Me_2NPh$, only a trace of the product was observed.

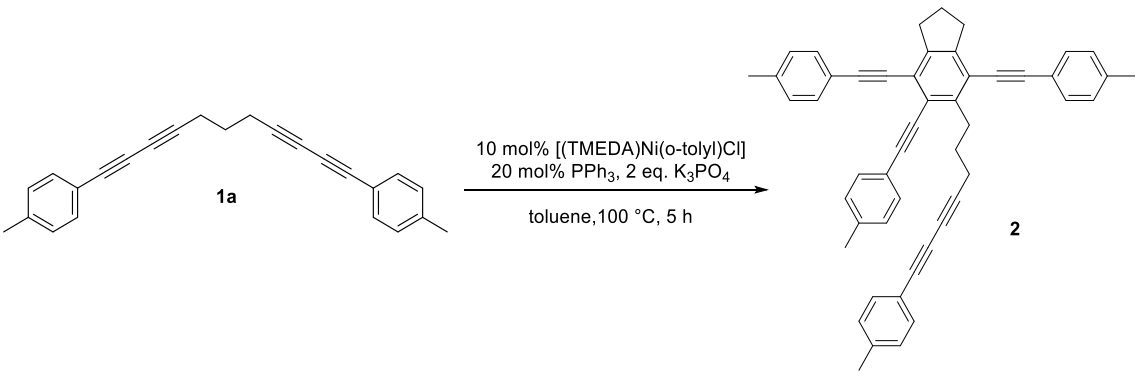

FIGURE 2 | Nickel-catalyzed bisdiyne cyclization reaction (18% isolated yield).

indane derivatives **5**, **6**, and **7** (Scheme 1), whereby the electron-rich linked bisdiyne significantly increased the yields of the reaction. To study the effect of an alternative donor moiety on the electrochemical and photophysical properties of the system, a bis(4-methoxyphenyl)aminophenyl-substituted linked bisdiyne was then combined with bis-4-cyanophenyl- and bis-4-pyridyl-substituted acetylenes, to generate compounds **8** and **9** (Scheme 1). Cyclization of the two inner alkynes of the linked bisdiyne with the added diarylacetylenes seems to be the preferred mode of reaction out of all possible ways in which the available triple bonds could cyclize. While the dimer of two linked bisdiynes was often detected as a minor side product, the cyclotrimerization of the diarylacetylenes was never observed under the conditions applied.

As noted in Scheme 1, some of the reactions were carried out in a microwave reactor for 2 h, whereas those conducted using an oil bath, at the same temperature, were run for 5 h. The yields of the procedure were low to moderate, as the conditions were not optimized for every combination of substituents, and some loss of product was encountered during column chromatography. When investigating the substrate scope, we noticed the following trend. The reaction only worked well when an electron-rich

27514765, 2026, 4, Downloaded from https://chemistry-europe.onlinelibrary.wiley.com/doi/10.1002/ceur.202500464 by Cochrane Croatia, Wiley Online Library on [24/11/2026]. See the Terms and Conditions (https://onlinelibrary.wiley.com/terms-and-conditions) on Wiley Online Library for rules of use; OA articles are governed by the applicable Creative Commons License

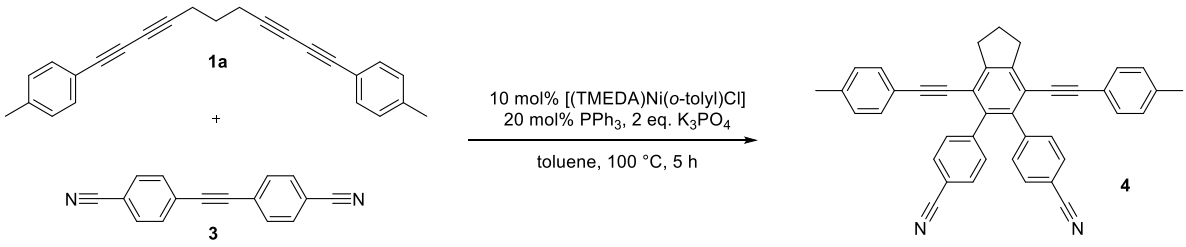

FIGURE 3 | Nickel-catalyzed linked bisdiyne-bis(4-cyanophenyl)acetylene cyclization reaction (20% isolated yield).

linked bisdiyne was combined with an electron-poor diarylacetylene. When combining linked bisdiynes and diphenylacetylenes with both components bearing the same substituent, either NMe_2 or nitrile, the desired tetra-*N*,*N*-dimethylaminophenyl-substituted derivative was not observed, while the tetra-cyanophenyl-substituted product was formed in <10% yield (Scheme 1, footnote). When the substitution pattern of the substrates was inverted, with the bisdiyne substrate bearing 4-cyanophenyl substituents and the diphenylacetylene bearing NMe_2 substituents, only a trace of the desired intermolecular cyclization product was observed (Scheme 1, footnote). In these unsuccessful attempts, the dimer formed from two linked bisdiyne molecules was detected in the mixtures, while the diarylacetylene component remained unreacted. When the reaction was conducted without the Ni-precatalyst, with all other reagents present, no reaction was observed. When the diphenylacetylene component was replaced with several different olefin derivatives, under the conditions used for the Ni-catalyzed cyclizations above, the formation of the respective cyclohexadiene derivatives was not observed (see Supporting Information). A test reaction, to reproduce the results using common conditions for cobalt-catalyzed [2 + 2 + 2] cyclizations, gave the desired bisdiyne-alkyne cyclo-co-trimerization product in trace amounts (Supporting Information) [59].

It is assumed that the reaction starts with the formation of a metallacyclopentadiene from reaction of Ni(0) with the linked bisdiyne. The metallacyclopentadiene can then insert another alkyne or undergo intermolecular or intramolecular Diels–Alder cyclization with another coordinated alkyne [53, 60–62]. While formal oxidative addition of the metal by formation of the metallacyclopentadiene is facilitated by an electron-rich bisdiyne, an electron-poor diarylacetylene likely favors the subsequent annulation. This would explain why the reaction only works well with certain substitution patterns, similarly to the Diels–Alder reaction, which favors electron-rich dienes and electron-poor dienophiles [63].

In order to obtain a water-soluble chromophore, compound **9** was treated with methyl triflate to afford the bistriflate salt **10,** with the color of the compound changing from yellow to red (Figure 4). The methylation occurs only on the pyridine and not on the triarylamine moieties, as confirmed via ^{15}N-HMBC spectroscopy (see Supporting Information). We previously explored the optical properties, cellular imaging, and binding to DNA's/RNA's of other conjugated *N*-methylpyridinium salts [64, 65].

2.2 | Single-Crystal X-Ray Diffraction

Compounds **4**, **5**, **6, 8**, and **9** were crystallized *via* vapor diffusion, and their structures were obtained *via* single-crystal X-ray diffraction (Figure 5 and Table 1). In the solid state, the aryl rings at the end of the alkynyl groups are somewhat twisted with respect to the central arene core, which is likely due to crystal packing forces, as the rotational barriers in solution are very small, giving rise to free rotation at room temperature [5, 66]. In all cases, the two aryl moieties located at *ortho*-positions on the central arene core, and formerly belonging to the diphenylacetylenes, are twisted with respect to the central arene ring as a result of steric interactions, with their interplanar angles with respect to the central ring being in the range 54.38(5)° – 71.60(5)°. The triphenylamine moieties of **8** and **9** exhibit a typical propeller-like shape, and the sums of the C–N–C angles around the amine nitrogen atoms in all compounds are very close to 360°, indicating a nearly trigonal planar environment around the N atoms.

2.3 | Photophysical Properties

2.3.1 | UV–vis and Fluorimetric Spectra

The photophysical properties of close analogs **4**, **5**, **6**, and **7** were compared. The spectra of **4**, which does not contain an amine

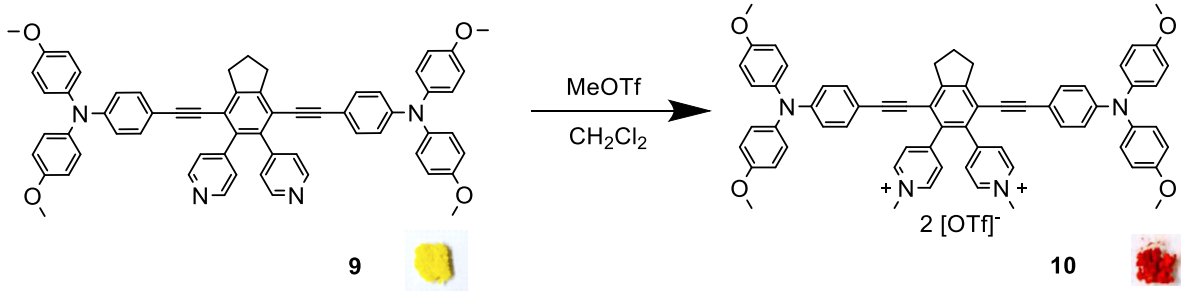

FIGURE 4 | Selective methylation of pyridine moieties in compound **9** to give **10,** along with pictures of the compounds as powders. The yield of **10** was 70%.

27514765, 2026, 4, Downloaded from https://chemistry-europe.onlinelibrary.wiley.com/doi/10.1002/ceur.202500464 by Cochrane Croatia, Wiley Online Library on [24/11/2026]. See the Terms and Conditions (https://onlinelibrary.wiley.com/terms-and-conditions) on Wiley Online Library for rules of use; OA articles are governed by the applicable Creative Commons License

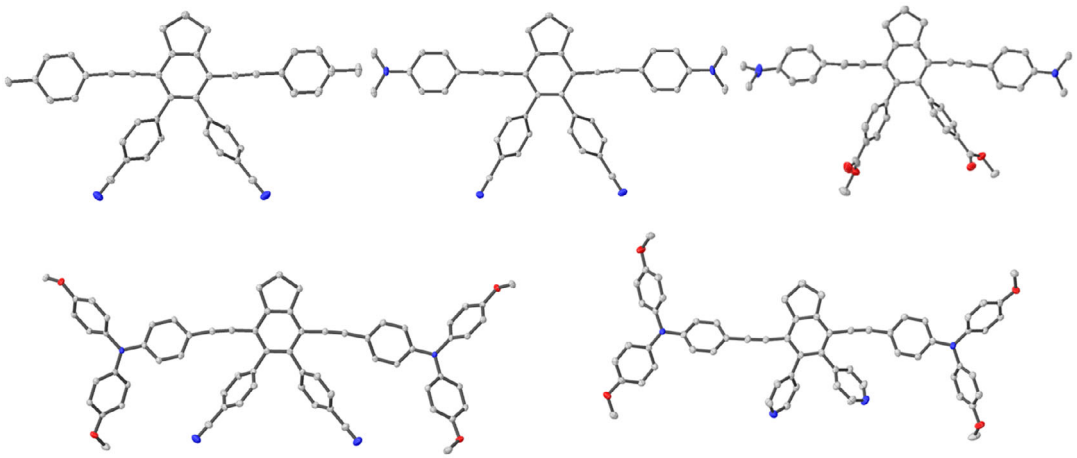

FIGURE 5 | Molecular structures of **4**, **5**, **6** (top row) and **8** and **9** (bottom row) with thermal ellipsoids drawn at the 50% probability level in the solid state. Hydrogen atoms are omitted for clarity. Nitrogen atoms are shown in blue and oxygen atoms in red.

TABLE 1 | Selected bond angles and interplanar angles (°) of **4**, **5**, **6**, **8**, and **9**. Ph = phenylene unit; end = at the end of the alkynyl moiety; cen = central; ortho = phenyl rings attached to the central phenyl ring.

			6[a]			
Compound	**4**	**5**	**mol 1**	**mol 2**	**8**[b]	**9**
Sum ∠ C–N–C		355.3(2), 360.0(2)	360.0(1), 355.4(2) /354.2(1)	360.0(1), 359.5(1) /359.7(2)	359.4(1) 2x	360.0(2), 360.0(2)
∠ Ph_{ortho}-Ph_{cen}	54.38(5), 60.27(5)	56.66(7), 54.11(7)	65.51(5), 71.60(5)	60.73(5), 68.34(5)	60.88(12) 2x	59.26(8), 65.08(8)
∠ Ph_{ortho}-Ph_{ortho}	66.23(6)	48.87(7)	58.87(5)	54.93(5)	68.75(5)	58.87(8)
∠ Ph_{end}-Ph_{cen}	27.49(4), 7.36(4)	14.98(6), 21.82(6)	19.93(5), 29.9(2) /62.3(2)	57.48(5), 26.3(1) /29.88(9)	22.69(6) 2x	12.58(7), 47.79(7)
∠ Ph_{end}-Ph_{end}	20.25(4)	36.80(6)	49.6(2) /82.2(2)	83.8(1) /30.62(8)	42.87(5)	35.27(7)

[a]There are two symmetry-independent molecules in the unit cell and values are given for both molecules. In addition, phenyl units at the ends of the alkynyl moieties of both molecules are disordered (ca. 50% occupancies) and values are given for both parts.
[b]The molecule has inversion symmetry.

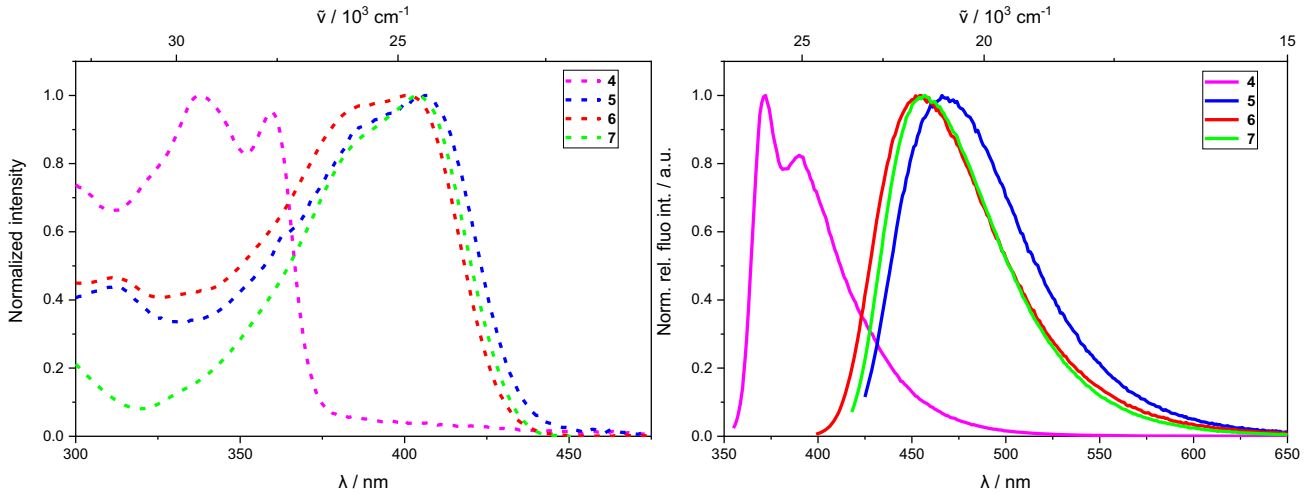

FIGURE 6 | Absorption (left) and emission (right) spectra of **4**, **5**, **6**, and **7** in CH_2Cl_2.

donor moiety, are drastically different from those of **5**, **6**, and **7**, with the latter donor–acceptor-donor compounds showing red-shifted absorption and broad, structureless emission bands, typical of charge–transfer (CT) behavior (Figure 6). In contrast, compound **4** displays vibrational fine structure, suggesting a locally excited (LE) state, even in CH_2Cl_2. The compounds

27514765, 2026, 4, Downloaded from https://chemistry-europe.onlinelibrary.wiley.com/doi/10.1002/ceur.202500464 by Cochrane Croatia, Wiley Online Library on [24/11/2026]. See the Terms and Conditions (https://onlinelibrary.wiley.com/terms-and-conditions) on Wiley Online Library for rules of use; OA articles are governed by the applicable Creative Commons License

exhibit good to excellent fluorescence quantum yields in nonpolar solvents and short fluorescence lifetimes in the nanosecond range (Table 2).

Absorption and emission spectra of **5**, **6**, and **7** were also recorded in solvents of different polarities, and the compounds exhibit significant solvatochromic fluorescence, typical of donor–acceptor systems which show enhanced CT character in polar solvents (Figures 7 and 8) [67, 68]. The emission redshift from toluene to MeCN is 3451 cm^{-1} for **5**, 3011 cm^{-1} for **6**, and 3256 cm^{-1} for **7**. Note that, although the compounds are formally D-A-D-type systems, the presence of acceptor groups at adjacent positions on the central phenyl ring leads to a permanent dipole moment.

Compounds **8** and **9**, bearing the strongly donating bis(4-methoxyphenyl)aminophenyl moieties, also exhibit strongly solvatochromic emission, with even larger redshifts from toluene to MeCN of 4520 cm^{-1} for **8** and 4563 cm^{-1} for **9**. They absorb strongly, with extinction coefficients of 83 000 $M^{-1}\,cm^{-1}$ (**8**) and 88 000 $M^{-1}\,cm^{-1}$ (**9**) in THF (Figures 9 and 10).

We further studied the photophysical properties of the dicationic compound **10** and found that it does not show any emission in solution. The bright red substance absorbs strongly in the UV and through the visible region of the spectrum, tailing beyond 600 nm in water, and its extinction coefficient is 73 000 $M^{1}\,cm^{-1}$ in THF (Figure 11). The lack of emission is likely due to the strength of the donor and acceptor moieties, which reduces the HOMO/LUMO gap and the S_1–S_0 energy gap. This may prevent fluorescence, as explained by the energy gap law, which states that the nonradiative decay rate (k_{nr}) of a transition increases exponentially with decreasing energy gap

TABLE 2 | Photophysical data of studied compounds in various solvents. Extinction coefficients were determined at the absorption band of lowest energy.

#	Solvent	ε, $M^{-1}\,cm^{-1}$	λ_{max} abs, nm	λ_{max} em, nm	Stokes shift, cm^{-1}	Φ_f	τ, ns	τ_0, ns	$k_{nr}/10^7 s^{-1}$	$k_r/10^7 s^{-1}$
4	CH_2Cl_2	34 000	340, 360	372, 390	900	0.67	3.00	4.5	11.0	22.3
5	Toluene		383, 398	438	2300	0.83	1.10	1.3	15.5	75.5
5	CH_2Cl_2	53 000	393, 406	468	3200	0.90	1.95	2.2	5.1	46.2
5	MeCN		390, 408	516	5100	0.38	3.27	8.6	19.0	11.6
6	Toluene		384, 401	427	1500	0.84	1.15	1.4	13.9	73.0
6	CH_2Cl_2	50 000	384, 401	455	3000	0.83	1.84	2.2	9.2	45.1
6	MeCN		384, 396	490	4800	0.50	2.84	5.7	17.6	17.6
7	*n*-Hexane		375, 395	407, 432	700	0.91	0.83	0.9	10.8	109.6
7	Toluene		386, 404	430	1500	0.97	0.92	0.9	3.3	105.4
7	THF	68 000	386, 402	459	3100	0.99	1.34	1.4	0.7	73.9
7	CH_2Cl_2		386, 402	456	3000	1	1.28	1.3	0.0	78.1
7	EtOH		386, 402	485	4300	0.17	0.4	2.4	207.5	42.5
7	MeCN		380, 397	500	5200	0.61	2.14	2.8	11.2	35.5
8	*n*-Hexane		293, 422	455	1700	0.86	1.42	1.7	9.9	60.6
8	Toluene		298, 423	472	2400	0.93	1.64	1.8	4.3	56.7
8	THF	83 000	293, 420	530	4900	0.95	3.04	3.2	1.6	31.3
8	CH_2Cl_2		289, 418	540	5400	0.86	3.18	3.7	4.4	27.0
8	EtOH		289, 415	551	5900	0.36	1.75	4.9	36.6	20.6
8	MeCN		293, 412	600	7600	0.16	0.96	6.0	87.5	16.7
9	*n*-Hexane		292, 417	442	1400	0.84	1.16	1.4	13.8	72.4
9	Toluene		295, 424	466	2100	1	1.44	1.4	0.0	69.4
9	THF	88 000	294, 418	525	4900	0.84	3.06	3.6	5.2	27.5
9	EtOH		291, 409	556	6500	0.26	1.18	4.5	62.7	22.0
9	MeCN		293, 417	595	7200	0.13	0.94	7.2	92.6	13.8
10	Toluene		370,435	—	—	—	—	—	—	—
10	THF	73 000	412	—	—	—	—	—	—	—
10	EtOH		396,430	—	—	—	—	—	—	—
10	MeCN		387, 426	—	—	—	—	—	—	—
10	Water		405, 470	—	—	—	—	—	—	—

27514765, 2026, 4, Downloaded from https://chemistry-europe.onlinelibrary.wiley.com/doi/10.1002/ceur.202500464 by Cochrane Croatia, Wiley Online Library on [24/11/2026]. See the Terms and Conditions (https://onlinelibrary.wiley.com/terms-and-conditions) on Wiley Online Library for rules of use; OA articles are governed by the applicable Creative Commons License

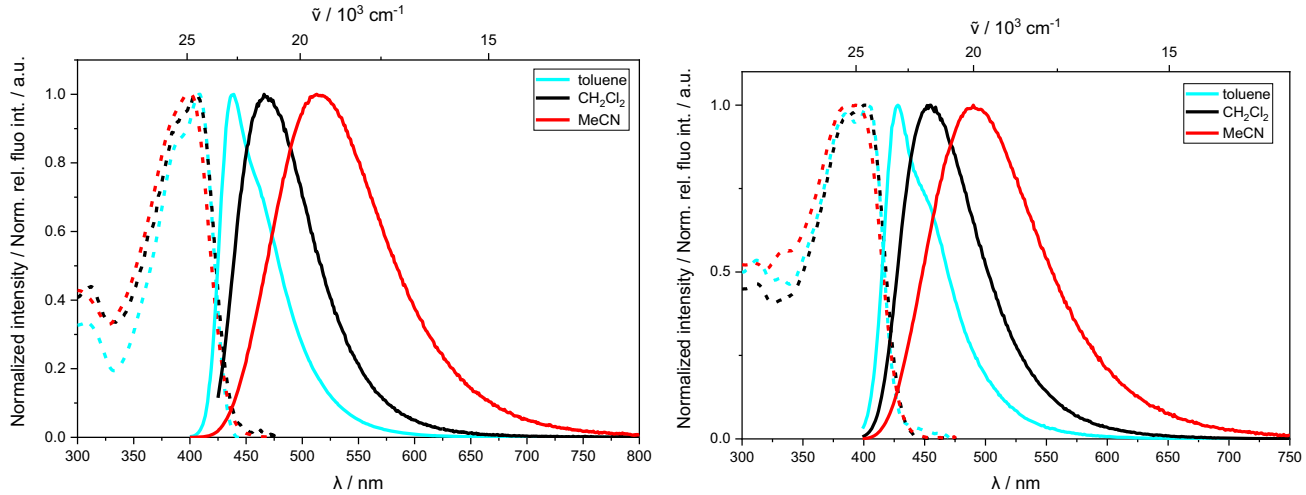

FIGURE 7 | Absorption (dashed) and emission (solid) spectra of **5** (left) and **6** (right) in three solvents.

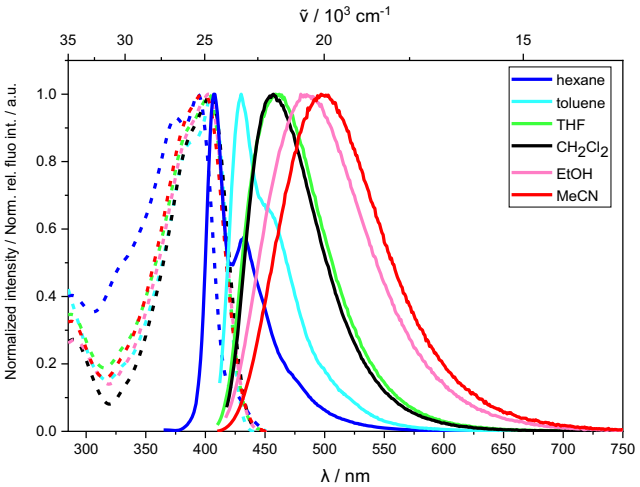

FIGURE 8 | Absorption (dashed) and emission (solid) spectra of **7** in six solvents.

between the two states [69–71]. Further discussion of the optical spectra of the various compounds in aqueous solution is given below in the section: *Photophysical studies of the new dyes in aqueous solutions.*

2.3.2 | Electrochemistry

Compounds **5** and **8** were studied using cyclic voltammetry (Figure 12). The values are given with respect to Fc/Fc^+ in THF. Compound **5** is irreversibly oxidized starting at 0.01 V and is irreversibly reduced in a multi-step process starting at −2.76 V. For **8**, irreversible oxidation occurs at 0 V, and a reduction was not observed within the solvent window. Both compounds bear two benzonitrile units as the acceptor moiety, with **5** having two dimethylaniline groups, while **8** bears two anisole groups on the amine nitrogen. While both compounds have similar oxidation behavior, the bis(4-methoxyphenyl)aniline groups shift the reduction potential of **8** significantly.

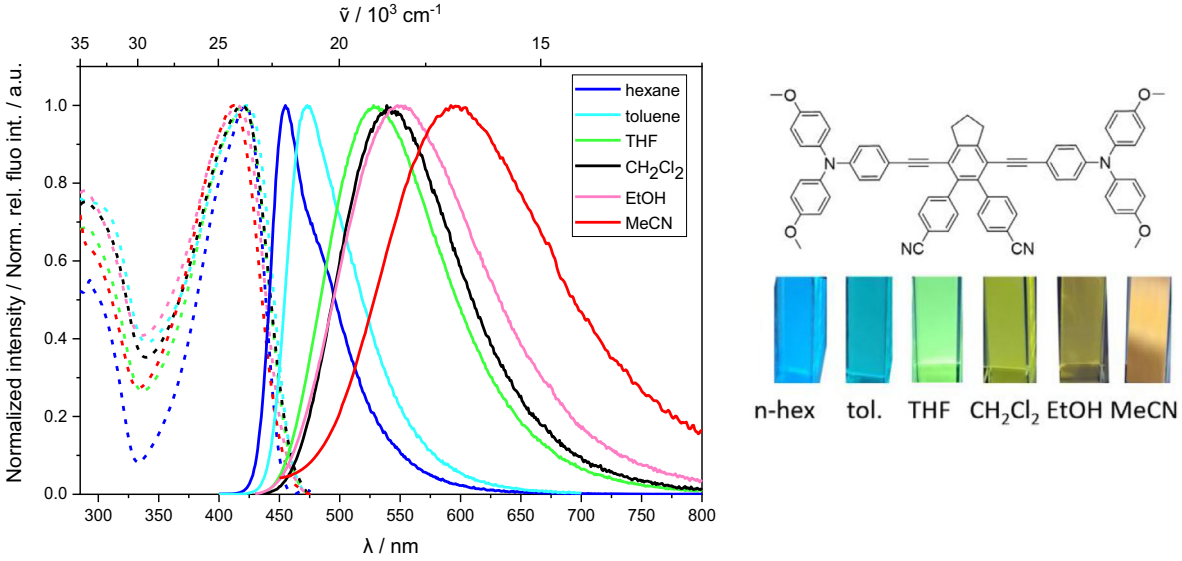

FIGURE 9 | Absorption (dashed) and emission (solid) spectra of **8** in solvents of different polarities and photos of the emission in cuvettes with an absorbance of 0.1, irradiated at 365 nm.

27514765, 2026, 4, Downloaded from https://chemistry-europe.onlinelibrary.wiley.com/doi/10.1002/ceur.202500464 by Cochrane Croatia, Wiley Online Library on [24/11/2026]. See the Terms and Conditions (https://onlinelibrary.wiley.com/terms-and-conditions) on Wiley Online Library for rules of use; OA articles are governed by the applicable Creative Commons License

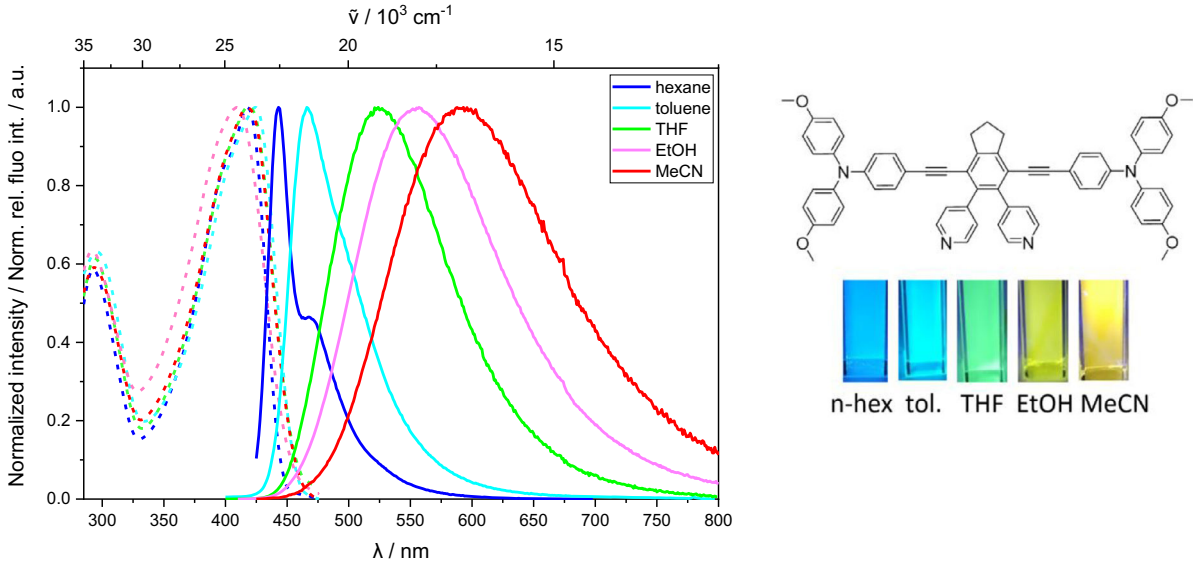

FIGURE 10 | Absorption (dashed) and emission (solid) spectra of **9** in solvents of different polarities and photos of the emission in cuvettes with an absorbance of 0.1, irradiated at 365 nm.

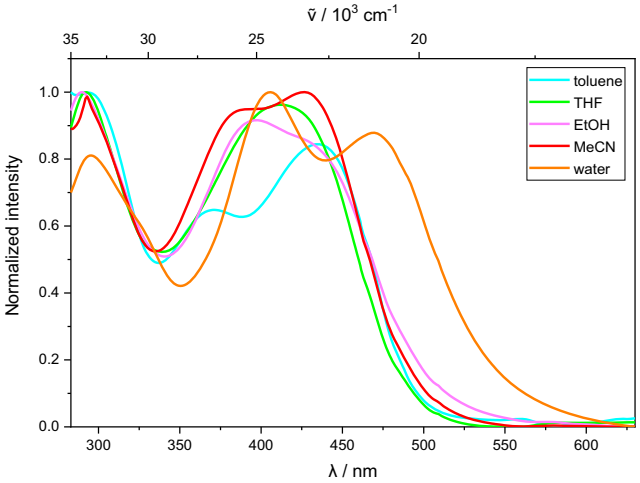

FIGURE 11 | Absorption spectra of **10** in solvents of different polarities.

2.3.3 | Vibrational Spectroscopy

The Raman and IR spectra of **8**, **9**, and **10** display aromatic C = C vibrations at ca. 1600 cm^{-1} and a characteristic C≡C stretch at 2194 cm^{-1} (Figure 13). The IR spectra of all compounds display C–H-stretches at 2750 cm^{-1} and above, which are not observed in the Raman spectra. The signals in the fingerprint area from 500 to 1500 cm^{-1} are much stronger than the rest of the spectrum in the IR-spectra in comparison to the Raman spectra. For **8**, the C≡N stretch vibration at 2226 cm^{-1} is visible in the Raman spectrum but much stronger in the IR spectrum in relation to the C≡C band (Figure 14). The IR intensity of aromatic nitriles is known to be enhanced when the molecule also bears electron-donating groups; furthermore, this vibration changes the dipole moment more than the polarizability [72]. The reverse is the case for the C≡C stretch, which is generally stronger in Raman spectra, and only significant in IR spectra when the moiety is located at the outer positions of a molecule [72]. Similar results were obtained from the IR and Raman spectra of **5** and **7** (Supporting Information, Figure S3).

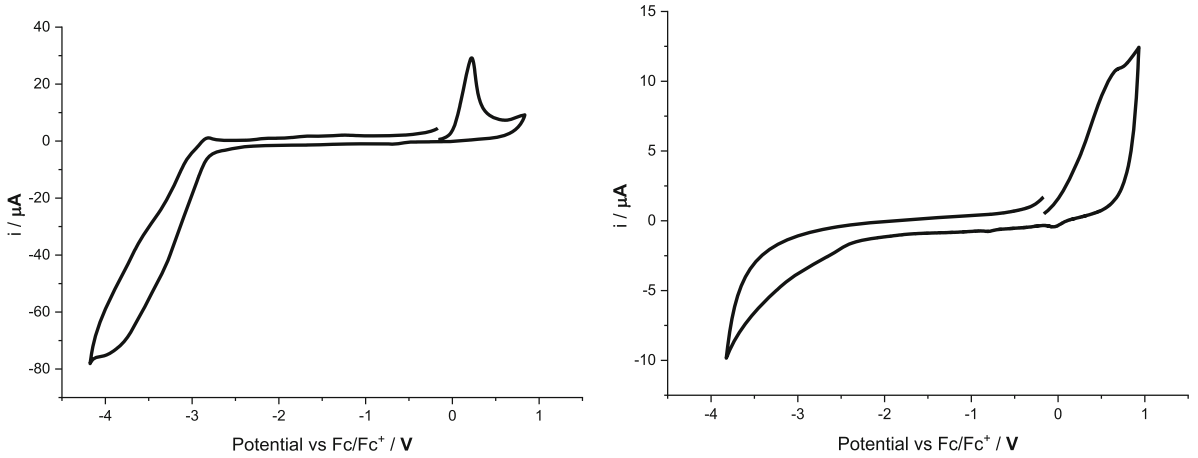

FIGURE 12 | Cyclic voltammograms of **5** (left) and **8** (right) in THF/0.1M [n-Bu_4N][PF_6].

27514765, 2026, 4, Downloaded from https://chemistry-europe.onlinelibrary.wiley.com/doi/10.1002/ceur.202500464 by Cochrane Croatia, Wiley Online Library on [24/11/2026]. See the Terms and Conditions (https://onlinelibrary.wiley.com/terms-and-conditions) on Wiley Online Library for rules of use; OA articles are governed by the applicable Creative Commons License

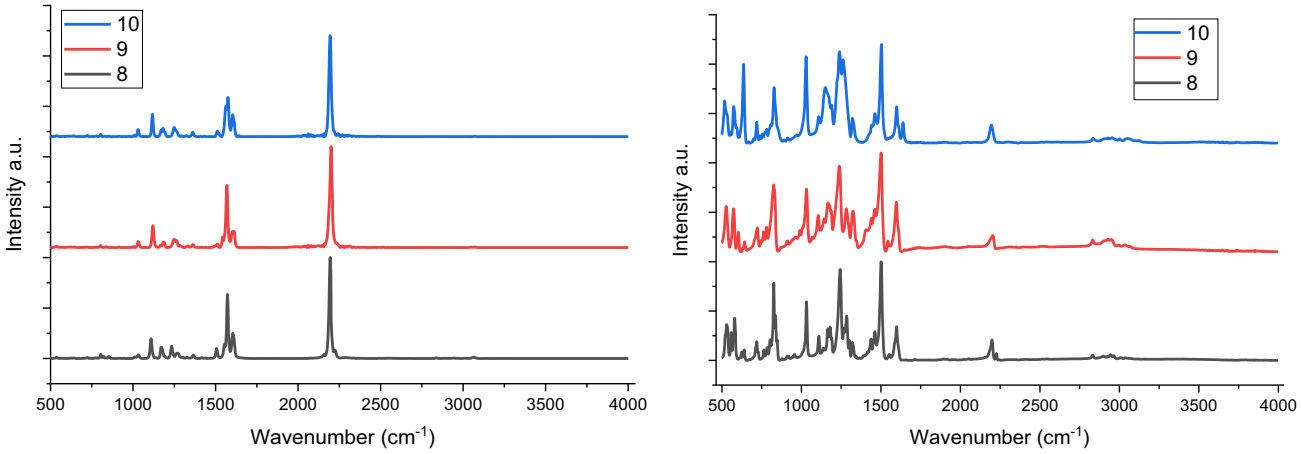

FIGURE 13 | Raman (left) and IR spectra (right) of **8**, **9**, and **10**.

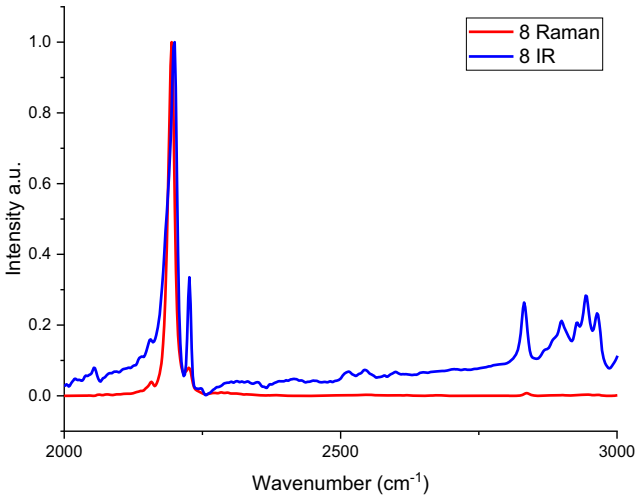

FIGURE 14 | Comparison of an excerpt of the Raman (red) and IR (blue) spectra of compound **8**, normalized to the C≡C stretching band.

2.4 | Interactions with DNA/RNA and Biorelevant Activity

2.4.1 | Photophysical Characterization of the New Dyes in Aqueous Solution

All compounds were dissolved in DMSO ($c = 2.5–10$ mM); such stock solutions were stored at +4°C, and working aliquots were kept at +25°C. No visible precipitation was observed in the working solutions. The UV–Vis spectra in aqueous solution (Figure 15a) are proportional to the concentration of dye up to $c = 4 \times 10^{-6}$ M (Supporting Information, Figures S4–S8), yielding a molar absorption coefficient (Table 3, ε). The results obtained do not support the formation of aggregates under the conditions used.

Detailed analysis of the UV-Vis spectra (Figure 15a) indicated a significant impact of the central indanyl core and thus the overall π conjugation length of the molecule on the overall spectral shape. While the absorption spectra of derivatives **5**, **8**, and **9** do not differ drastically, **1c**, lacking a central aryl unit, revealed a pronounced hypsochromic shift of its absorption maximum ($\Delta\lambda > 40$ nm) compared to **5**, **8**, and **9**. Compared to the other compounds studied, the biggest difference in spectral shape

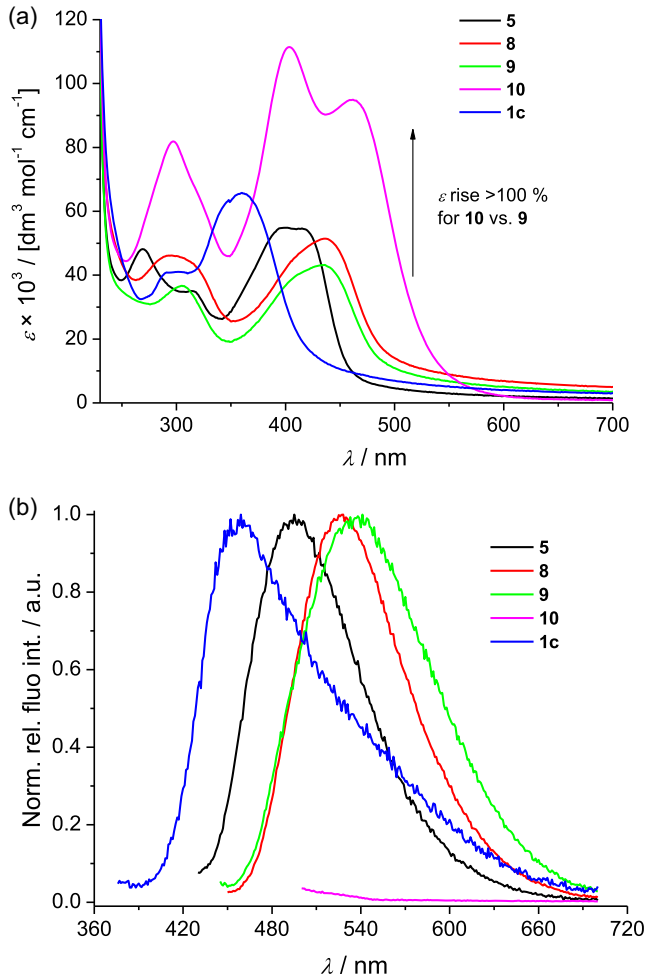

FIGURE 15 | (a) Comparison of the UV-Vis spectra of the novel dyes in aqueous solution; (b) normalized fluorescence spectra of the dyes at $c = 2.0 \times 10^{-6}$ M. Note negligible emission of **10**, even at the highest sensitivity of the instrument.

and intensity is observed for **10**, the *N*-methylated analog of **9**, which differs only in terms of the enhanced acceptor strength of the *N*-methylpyridinium substituents (R_2) (Table 3). It reveals the highest absorptivity and much better resolved spectral bands than its neutral analog **9**.

27514765, 2026, 4, Downloaded from https://chemistry-europe.onlinelibrary.wiley.com/doi/10.1002/ceur.202500464 by Cochrane Croatia, Wiley Online Library on [24/11/2026]. See the Terms and Conditions (https://onlinelibrary.wiley.com/terms-and-conditions) on Wiley Online Library for rules of use; OA articles are governed by the applicable Creative Commons License

TABLE 3 | Spectrophotometric data of the dyes in aqueous solution at pH 7.0, sodium cacadolyte buffer, $I = 0.05$ M.

Compound	$^{max}\lambda_{Abs}$, nm	ε [$\times 10^4$ M^{-1} cm^{-1}]	$^{max}\lambda_{Em}$, nm	$\Delta\tilde{\nu}$, cm^{-1}[a]	Φ_f[b] %
5	418	5.56	495	3721	5.3
8	436	5.25	527	3960	19.3
9	435	4.25	537	4367	1.8
10	462	8.92	—[c]	—[c]	—[c]
1c	360	6.49	459	5991	

[a]$\Delta\tilde{\nu} = {}^{max}\lambda_{Em} - {}^{max}\lambda_{Abs.}$
[b]Quantum yield in deionized water.
[c]Compound has negligible intrinsic fluorescence.

The fluorescence emission maxima of most of the studied dyes follow the shifting trend observed for their UV-Vis maxima (Figure 15a vs. Figure 15b). Only derivative **10** showed negligible fluorescence emission (Supporting Information, Figure S12). All compounds possessing intrinsic emission in aqueous buffer solution (**5**, **8**, **9**, and **1c**) exhibit significant Stokes shifts ranging from 3721 to 5991 cm^{-1} (Table 3). The emission intensity of all dyes was proportional to concentration within the 5×10^{-7} – 2×10^{-6} M range (Supporting Information, Figures S9a, S10a, S11a, and S13a), pointing to the absence of any dye aggregation.

The spectra of all emissive dyes revealed a hypochromic effect upon heating within the 25°C to 95°C temperature range, as well as a hypsochromic effect in the cases of **5** and **8** (Supporting Information, Figures S9b, S10b, S11b, and S13b). Additionally, compounds **8** and **9** showed excellent reproducibility upon reversible cooling of the sample solutions (Supporting Information, Figures S10b and S11b), while compounds **5** and **1c** revealed irreversibly suppressed emission spectra (Supporting Information, Figures S9b and S13b).

2.4.2 | Interactions of New Dyes with Ds-DNA and Ds-RNA

Interactions of sterically demanding small molecules with ds-DNA or ds-RNA are often strongly dependent on polynucleotide secondary structure; therefore, we used several ds-DNA or ds-RNA with distinct structural features (Supporting Information, Table S4).

2.4.3 | Spectrophotometric Titrations of the New Dyes with Polynucleotides

2.4.3.1 | **Fluorimetric Titrations.** The strong emission and favorable Stokes shifts of the emission maxima allowed us to perform fluorimetric titrations of the dyes with ds-DNA and ds-RNA at very low (50 nM) concentrations. In general, the addition of any ds-DNA or ds-RNA to the dyes resulted in pronounced hypochromic and hypsochromic shifts of the emission maxima (Figure 16, Supporting Information, Figures S14–S29).

In most fluorimetric titrations, the presence of isosbestic points strongly supported the formation of only one dominant type of dye/polynucleotide complex (e.g., Supporting Information, Figure S22). The titration data were processed by a nonlinear fitting procedure to the Scatchard equation [73–75], yielding binding constants (Table 4, Supporting Information, Figures S14–S29).

Although the emission of each dye is uniformly quenched by all ds-DNA and ds-RNA samples (Figure 17a–d), variations in quenching efficiency and binding affinity were observed among the studied compounds. Specifically, the dimethylamino-substituted derivative **5** exhibited a slightly higher affinity toward ctDNA and poly(dGdC)$_2$, showing over a 50% decrease in emission (Figure 17a,d). In contrast, the bis(4-methoxyphenyl)

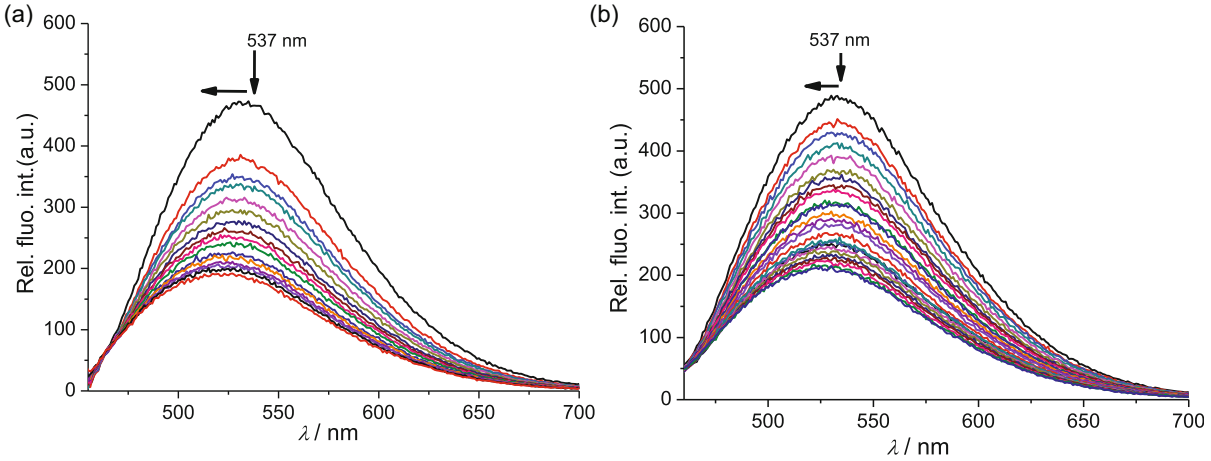

FIGURE 16 | Changes in the fluorescence spectrum of **9** ($c = 5.0 \times 10^{-8}$ M) upon titration with: (a) poly A-poly U, and (b) poly(dAdT)$_2$ ($\lambda_{exc} = 435$ nm, $\lambda_{em} = 537$ nm). Measured in sodium cacodylate buffer, pH 7.0, $I = 0.05$ M.

27514765, 2026, 4, Downloaded from https://chemistry-europe.onlinelibrary.wiley.com/doi/10.1002/ceur.202500464 by Cochrane Croatia, Wiley Online Library on [24/11/2026]. See the Terms and Conditions (https://onlinelibrary.wiley.com/terms-and-conditions) on Wiley Online Library for rules of use; OA articles are governed by the applicable Creative Commons License

TABLE 4 | Binding constants ([a]logK_s) and emission quenching efficiency ([b]ΔInt) of complexes of the dyes with ds-polynucleotides calculated by processing the fluorimetric titrations at pH = 7.0, sodium cacodylate buffer, $I = 0.05$ M.

	[a]log K_s, [b]ΔInt			
Compound	**ctDNA**	**poly A-poly U**	**p(dAdT)$_2$**	**p(dGdC)$_2$**
5	7.7 (0.43)	7.4 (0.58)	8.1 (0.76)	7.4 (0.46)
8	8.1 (0.68)	7.7 (0.80)	7.2 (0.58)	7.2 (0.63)
9	7.7 (0.62)	7.9 (0.40)	7.3 (0.42)	7.5 (0.57)
10	/	/	[c]7–8	/
1c	6.9 (0.70)	7.5 (0.65)	6.8 (0.46)	7.1 (0.69)

[a]Processing of fluorimetric titration data employing the Scatchard equation [73–75]. For easier comparison, all log K_s values were recalculated for fixed n[bound dye]/ [polynucleotide] = 0.2. The correlation coefficients were >0.99 for all calculated K_s [76].
[b]$\Delta Int = Int_{(100\%\ complex)}/Int_0$.
[c]Estimated from $IDA_{50\%}$ (Figure 20).

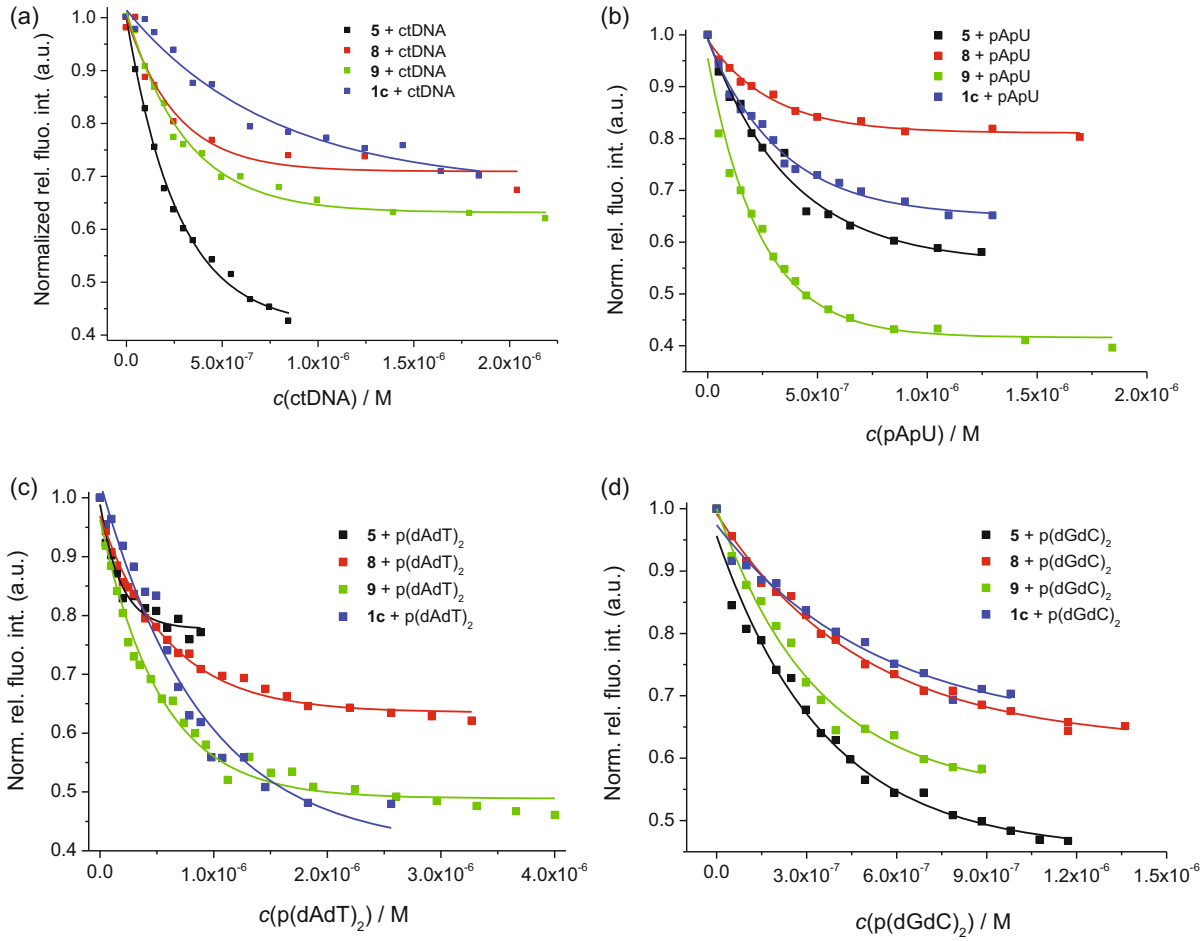

FIGURE 17 | Normalized fluorescence intensities of **5**, **8**, **9**, and **1c** (c(**dye**) = 5.0×10^{-8} M) upon titration with polynucleotides: (a) ctDNA; (b) poly A-poly U; (c) p(dAdT)$_2$, and (d) p(dGdC)$_2$). Measured in sodium cacodylate buffer, pH 7.0, $I = 0.05$ M.

aminophenyl-substituted derivative **9** demonstrated greater emission selectivity toward poly A–poly U and poly(dAdT)$_2$ sequences, also with emission decreases of at least 50% (Figure 17b,c).

The remarkably high but similar values of the binding constants (log $K_s \geq 7$–8) (Table 4) obtained from the fluorimetric titrations for all ds-polynucleotides studied suggest a generally high affinity of tested dyes with no significant preference toward any specific ds-DNA or ds-RNA secondary structure.

2.4.3.2 | Indicator Displacement Assay (IDA) Experiments. The high stability constants for dye/polynucleotide complexes in the case of **5**, **8**, **9**, and **1c** prompted us to investigate further the potential of **10,** with negligible intrinsic fluorescence. In principle, the emission from **10** could increase upon the addition of DNA/RNA; however, in the experiment, no change was observed. We also performed UV/Vis titrations of **10** with ds-DNA and ds-RNA, which yielded a clear hypochromic effect and broadening of the absorption maxima (Supporting

27514765, 2026, 4, Downloaded from https://chemistry-europe.onlinelibrary.wiley.com/doi/10.1002/ceur.202500464 by Cochrane Croatia, Wiley Online Library on [24/11/2026]. See the Terms and Conditions (https://onlinelibrary.wiley.com/terms-and-conditions) on Wiley Online Library for rules of use; OA articles are governed by the applicable Creative Commons License

Information, Figure S31); however, a small number of titration points did not allow accurate calculation of binding constants.

This directed us to use an alternative indicator displacement assay (IDA) methodology [77–79], particularly an ethidium bromide (EtBr) displacement assay, by preparing a highly emissive EtBr/polynucleotide complex and then displacing EtBr by addition of **10** while monitoring the decrease of EtBr emission (Figure 18a) [78, 79].

The results obtained indicate the ability of **10** to displace EtBr from p(dAdT)$_2$; however, regarding the calculated IDA$_{50\%}$ value (IDA$_{50\%}$ = [EtBr] / [**10**] at which 50% of EtBr is displaced) (Figure 18b), its affinity for the AT-DNA sequence is much lower than that of EtBr. Taking into account that EtBr is known as an intercalator, which is, in this case, displaced by **10**, whose mode of binding was not yet elucidated, we performed additional competition experiments with 4′, 6-diamidino-2-phenylindole (DAPI). DAPI is a typical minor groove binder, highly selective for the AT-DNA minor groove, and for monitoring displacement, we opted for circular dichroism (CD) as a fluorescence-independent method (see discussion below for **10**).

2.4.3.3 | Circular Dichroism (CD) Experiments. To investigate the binding of dyes to ds-DNA/RNA in more detail, we used CD spectroscopy, a useful analytical tool in the binding study of small molecules to chiral macromolecules [80]. Small molecules can, upon binding, change the helical chirality of ds-DNA/RNA (observed as a change in spectral region $\lambda < 300$ nm), and achiral molecules can, upon binding to chiral DNA/RNA, acquire induced chirality (observed as an induced (I)CD signal(s) positioned at the absorption bands of the small molecule). All such changes provide information on the binding mode (intercalation, agglomeration, groove binding, etc.) to a polynucleotide [81, 82].

It should be noted that under the experimental conditions, all compounds studied are achiral (Supporting Information, Figure S35), thus not interfering with the monitoring of the CD spectral properties of the polynucleotides investigated.

The addition of some dyes (**5**, **9**, **1c**) to ds-DNA or ds-RNA did not cause a significant change in the CD spectrum of the polynucleotides (spectral region $\lambda < 300$ nm) (Supporting Information, Figures S36, S38, S40), confirming the preservation of the helicity of the DNA/RNA. However, compound **8** caused a minor decrease in ds-DNA bands (Supporting Information, Figure S37).

Notably, the addition of compound **10** to ds-DNA/RNA resulted in a pronounced reduction of DNA/RNA helicity (Figure 19; Supporting Information, Figure S39). Furthermore, a distinct but weak negative induced CD (ICD) band was detected between 430–500 nm, corresponding to the longest-wavelength absorption band of **10** ($\lambda = 462$ nm) in the complex with ctDNA (Figure 19a), and a positive one with poly(dAdT)$_2$ (Figure 19b). These findings indicate a uniform orientation of the chromophore **10** relative to the chiral axis of double-stranded polynucleotide [81, 82]. The opposite sign of the ICD band of **10** can be attributed to the different secondary structures (Supporting Information, Table S4) of ct-DNA (B-helix with minor groove commonly interacting with small molecules) and ds-RNA (A-helix, major groove commonly interacting with small molecules), whereby compound **10** adopts different orientations in grooves, depending on the groove width and depth (Supporting Information, Table S4). This distinctive CD response of the **10**/DNA(RNA) complexes compared to other neutral analogs likely arises from the unique nature of this permanently positively charged compound, where electrostatic interactions of **10** with the anionic DNA/RNA backbone induce both helicity alterations and consistent chromophore alignment.

To examine the mode of binding of cationic derivative **10** in more detail, we performed a displacement experiment with a well-known minor groove binder DAPI. DAPI binds into the AT-DNA minor groove with high affinity, yielding a strong positive ICD band at ca. 375 nm [83]. If cationic derivative **10** also binds into the DNA minor groove, it should efficiently displace DAPI; however, if it binds into the major groove, the DAPI ICD band should remain unchanged [84]. Indeed, the addition of **10** very efficiently displaced DAPI, as monitored by the disappearance of the DAPI ICD band (Figure 20a). The observed IDA$_{50\%}$ value suggests an almost identical affinity of derivative **10** for the AT-DNA minor groove as that of DAPI [85] (IDA$_{50\%}$ = [DAPI] / [**10**] = 1.1) (Figure 20b); thus, the binding affinity of **10** toward AT-DNA sequences can be estimated within the range $K_s = 10^7$–10^8 M^{-1} (Table 4).

Due to the different binding modes of EtBr (DNA intercalator, see Figure 18) and DAPI (DNA minor groove binder), mutual comparison of IDA$_{50\%}$ values obtained from these two

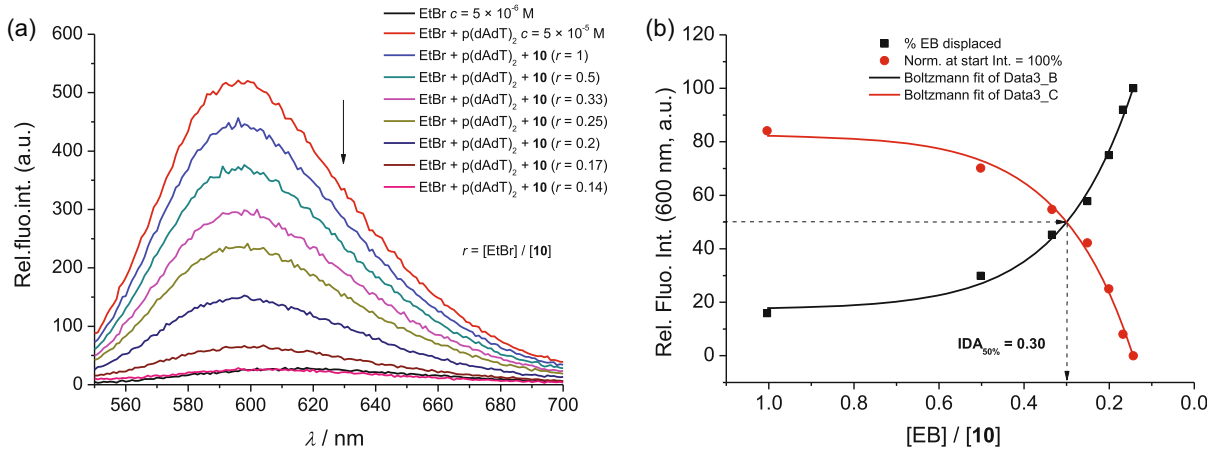

FIGURE 18 | Changes in the fluorescence of ethidium bromide ($c = 5 \times 10^{-6}$ M, $\lambda_{exc} = 520$ nm, $\lambda_{em} = 600$ nm) from the complex with p(dAdT)$_2$ ($c = 5 \times 10^{-5}$ M) upon addition of **10**. Measured in sodium cacodylate buffer, pH 7, $I = 0.05$ M.

27514765, 2026, 4, Downloaded from https://chemistry-europe.onlinelibrary.wiley.com/doi/10.1002/ceur.202500464 by Cochrane Croatia, Wiley Online Library on [24/11/2026]. See the Terms and Conditions (https://onlinelibrary.wiley.com/terms-and-conditions) on Wiley Online Library for rules of use; OA articles are governed by the applicable Creative Commons License

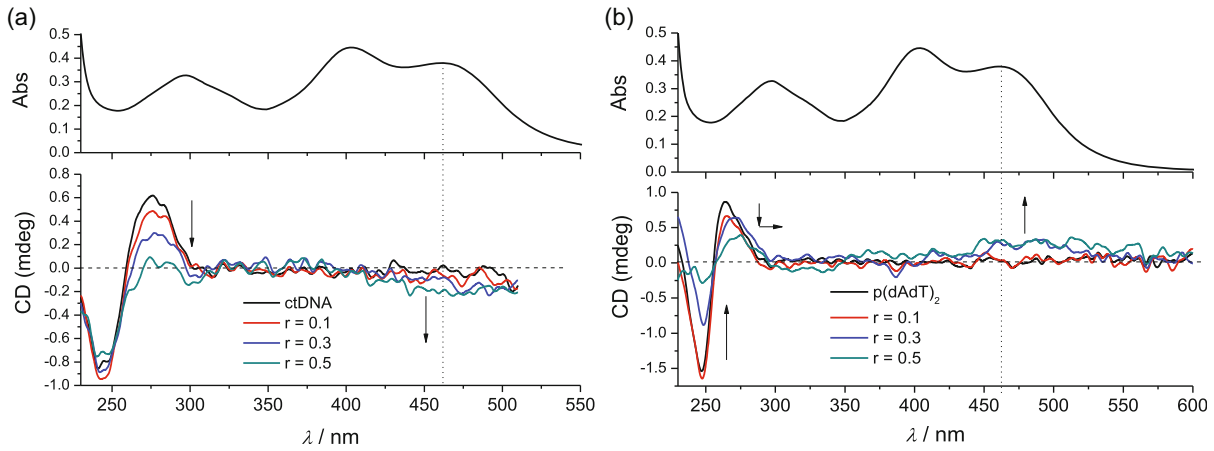

FIGURE 19 | CD titration of: a) ctDNA ($c = 1 \times 10^{-5}$ M) and b) poly A-poly U ($c = 1 \times 10^{-5}$ M) with **10** at molar ratios r = [compound] / [polynucleotide]. Measured in sodium cacodylate buffer, pH 7, $I = 0.05$ M.

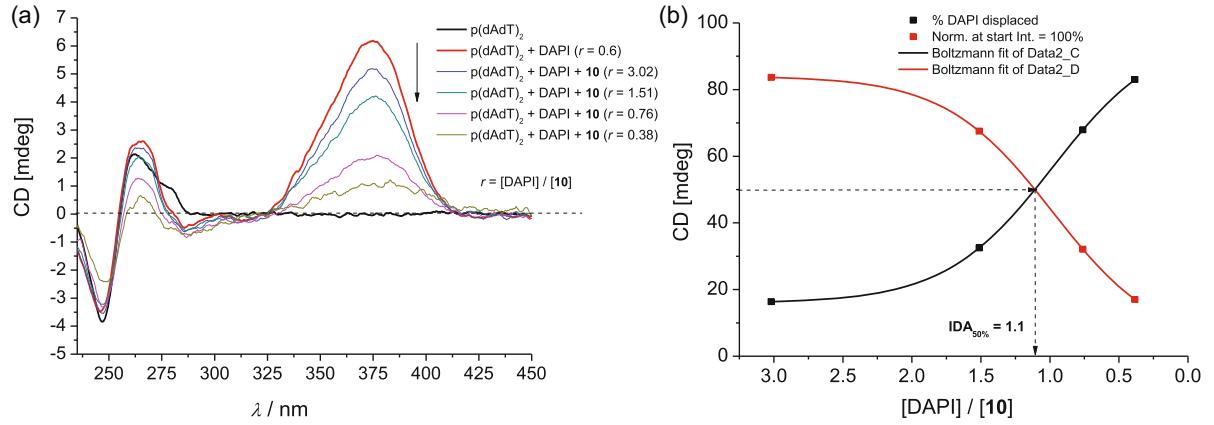

FIGURE 20 | DAPI ($c = 1.2 \times 10^{-5}$ M) displacement with **10** after binding to p(dAdT)$_2$ ($c = 2 \times 10^{-5}$ M). Done in sodium cacodylate buffer (pH = 7.0, $I = 0.05$ M).

independent experiments suggests minor groove binding as a prevalent mode of interaction of **10** with AT-DNA, agreeing well with the aforementioned binding mode to ct-DNA.

2.4.3.4 | Thermal Denaturation of Ds-DNA/RNA. Thermal denaturation experiments provide information about the ds-polynucleotide helix thermal stability as a function of its interaction with added small molecules [86]. The difference between the T_m value of free ds-polynucleotide and a complex with a small molecule (ΔT_m value) is an important factor in the characterization of small molecule/ds-polynucleotide interactions. Moderate to strong stabilization ($\Delta T_m > 5$°C) supports pronounced intercalative or minor groove binding interaction [87, 88]. In contrast, weak or negligible stabilization ($\Delta T_m = 0$–5°C) suggests a binding process driven mostly by hydrophobic effects accompanied by weak H-bonding and/or electrostatic interactions, usually excluding classical intercalation as a binding mode.

The addition of our studied dyes to ds-DNA or ds-RNA resulted mostly in weak or even negligible impact on the stability of ds-helices (Supporting Information, Table S4, Figures S32–S34). This agrees well with the aforementioned CD results, which show that studied compounds bind within grooves of ds-DNA or ds-RNA, relying dominantly on the hydrophobic or VdW attractive forces, with the exception of additional electrostatic interactions of cationic analog **10**.

2.5 | Biological Effects of 5, 8, 9, 10, and 1c on a Human Cell Line

Prior experiments in this work showed that the studied dyes strongly bind to ds-DNA/RNA, which could potentially cause strong cytotoxicity [88]. Thus, we studied the impact of the

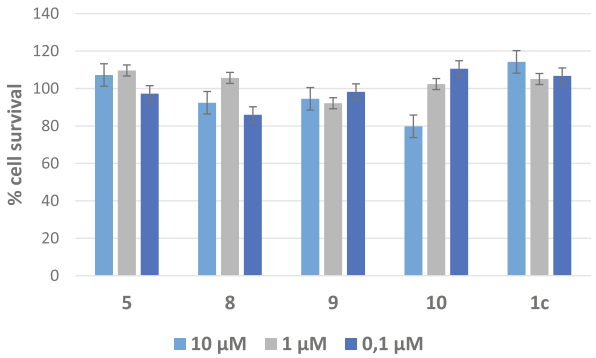

FIGURE 21 | Cell survival of A549 cells treated with different concentrations of all studied dyes. Data are presented as mean ± SD made in four replicates, relative to the control samples. Control samples consist of cells treated with DMSO at the same concentration as the compound tested. Representative data from three independent experiments, which yielded similar results, are shown.

27514765, 2026, 4, Downloaded from https://chemistry-europe.onlinelibrary.wiley.com/doi/10.1002/ceur.202500464 by Cochrane Croatia, Wiley Online Library on [24/11/2026]. See the Terms and Conditions (https://onlinelibrary.wiley.com/terms-and-conditions) on Wiley Online Library for rules of use; OA articles are governed by the applicable Creative Commons License

addition of our dyes on the cell viability of the human lung carcinoma cell line (A549) by the MTT assay (Figure 21). Compared to the control cells (cells treated with DMSO, which was used as a diluent for the dyes), cells treated with the studied compounds exhibited a negligible decrease in cell survival even at the highest concentration tested (10 μM).

3 | Conclusions

Nickel(0)-catalyzed [2 + 2 + 2] cycloadditions of linked bisdiynes with diarylacetylenes were conducted, using the Ni(II) catalyst precursor [(TMEDA)Ni(*o*-tolyl)Cl] as the Ni(0) source, to which two equivalents of PPh_3 per Ni were added. The reaction works best with bisdiynes bearing electron-donating groups and diarylacetylenes bearing electron-accepting substituents. The resulting air-stable, approximately C_{2v}-symmetric D-π-A-π-D *o*-terphenyl dyes were studied by UV/Vis and fluorescence spectroscopy. Spectroscopic analyses revealed strongly solvatochromic emission with high quantum yields in solution, except for the non-emissive *N*-methylpyridinium derivative, the latter pointing toward the decisive impact of pyridine methylation on the non-radiative relaxation of the fluorophore. The vibrational spectra of the triarylamine dyes show a strong characteristic alkyne stretching band in the Raman and IR spectra.

Biorelevant studies demonstrated that the examined dyes exhibit strong interactions with double-stranded DNA and RNA, most likely through groove insertion, which results in pronounced fluorescence quenching. Among them, only the dicationic derivative **10** displayed a distinct CD response upon binding, attributed to additional electrostatic interactions with the nucleic acid backbone that orient the dye specifically within the binding site, likely the DNA minor groove or RNA major groove. The dyes showed negligible influence on polynucleotide thermal stability, indicating that their binding is primarily governed by hydrophobic and van der Waals forces, with the exception of derivative **10**, which also involves electrostatic contributions. Moreover, all compounds exhibited negligible cytotoxicity toward human cell lines. These results, combined with our prior reports [21, 22], justify pursuing more detailed investigations into these dyes as multimodal fluorescence, CD, and Raman (SERS) probes for detecting DNA/RNA content in both intracellular and extracellular bioimaging applications.

Crystal Structures

Deposition Numbers 2 497 286 (**4**), 2 497 287 (**5**), 2 497 288 (**6**), 2 497 289 (**8**), and 2 497 290 (**9**) contain the supplementary crystallographic data for this paper. These data are provided free of charge by the joint Cambridge Crystallographic Data Centre and Fachinformationszentrum Karlsruhe Access Structures service.

Author Contributions

Synthesis and characterization of new compounds: RR; assistance with the synthesis of new compounds: SL, JS, AN, and MK; X-ray crystallography: JK, FK, and AF; Cyclic voltammetry: LZ; Raman spectroscopy: NS; study of interactions with biomacromolecules: NV and DPS; biological testing: LLH; conceptualization, supervision, funding acquisition, writing of the manuscript: MF, DPS, IP, and TBM. All authors have read and agreed to the published version of the manuscript.

Acknowledgments

TBM thanks the Julius-Maximilians-Universität Würzburg for support. Part of this work was supported by the Croatian Science Foundation under the project number HrZZ IP-2022-10−9829.

Funding

This study was supported by Julius-Maximilians-Universität Würzburg, Croatian Science Foundation (HrZZ IP-2022-10−9829).

Conflicts of Interest

The authors declare no conflicts of interest.

Data Availability Statement

The data that support the findings of this study are available in the Supporting Information of this article.

References

1. U. H. F. Bunz, "Poly(aryleneethynylene)s: Syntheses, Properties, Structures, and Applications," *Chemical Reviews* 100 (2000): 1605.

2. U. H. F. Bunz, "Poly(aryleneethynylene)s," *Macromolecular Rapid Communications* 30 (2009): 772.

3. U. H. F. Bunz, Y. Rubin, and Y. Tobe, "Polyethynylated Cyclic π-Systems: Scaffoldings for Novel Two and Three-Dimensional Carbon Networks," *Chemical Society Reviews* 28 (1999): 107.

4. A. Beeby, K. S. Findlay, P. J. Low, et al., "Studies of the S_1 State in a Prototypical Molecular Wire Using Picosecond Time-Resolved Spectroscopies," *Chemical Communications* (2003): 2406.

5. A. Beeby, K. Findlay, P. J. Low, and T. B. Marder, "A Re-Evaluation of the Photophysical Properties of 1,4-Bis(phenylethynyl)benzene: A Model for Poly(phenyleneethynylene," *Journal of the American Chemical Society* 124 (2002): 8280.

6. H. Huy Do, A. Villinger, S. Lochbrunner, P. Ehlers, and P. Langer, "Palladium-Catalyzed Synthesis and Fluorescence Study of Ethynylated Naphthalene Derivatives," *European Journal of Organic Chemistry* 2017 (2017): 2238.

7. M. Lübtow, I. Helmers, V. Stepanenko, R. Q. Albuquerque, T. B. Marder, and G. Fernández, "Self-Assembly of 9,10-Bis (phenylethynyl) Anthracene (BPEA) Derivatives: Influence of π–π and Hydrogen-Bonding Interactions on Aggregate Morphology and Self-Assembly Mechanism," *Chemistry – A European Journal* 23 (2017): 6198.

8. B. Breiten, I. Biaggio, and F. Diederich, "Nonplanar Push–pull Chromophores for Opto-Electronic Applications," *Chimia* 64 (2010): 409.

9. J. Zhang, Z. C. Smith, and S. W. Thomas, "Electronic Effects of Ring Fusion and Alkyne Substitution on Acene Properties and Reactivity," *Journal of Organic Chemistry* 79 (2014): 10081.

10. P. Nguyen, S. Todd, D. Van den Biggelaar, et al., "Facile Route to Highly Fluorescent 9,10-Bis(p-R-Phenylethynyl)anthracene Chromophores via Palladium/Copper Catalyzed Cross-Coupling," *Synlett* 1994 (1994): 299.

11. F. Diederich, P. J. Stang, and R. R. Tykwinski, *Acetylene Chemistry: Chemistry, Biology and Material Science* (John Wiley & Sons, 2006).

12. S. M. Berger and T. B. Marder, "Applications of Triarylborane Materials in Cell Imaging and Sensing of Bio-Relevant Molecules Such as DNA, RNA, and Proteins," *Materials Horizons* 9 (2022): 112.

27514765, 2026, 4, Downloaded from https://chemistry-europe.onlinelibrary.wiley.com/doi/10.1002/ceur.202500464 by Cochrane Croatia, Wiley Online Library on [24/11/2026]. See the Terms and Conditions (https://onlinelibrary.wiley.com/terms-and-conditions) on Wiley Online Library for rules of use; OA articles are governed by the applicable Creative Commons License

13. M. Ferger, C. Roger, E. Köster, et al., "Electron-Rich EDOT Linkers in Tetracationic Bis-Triarylborane Chromophores: Influence on Water-Stability, Bio-Macromolecule Sensing, and Photoinduced Cytotoxicity," *Chemistry – A European Journal* 28 (2022): e202201130.

14. S. M. Berger, J. Rühe, J. Schwarzmann, et al., "Bithiophene-Cored, *Mono*-, *Bis*-, and *Tris*-(Trimethylammonium)-Substituted, *Bis*-Triarylborane Chromophores: Effect of the Number and Position of Charges on Cell Imaging and DNA/RNA Sensing," *Chemistry – A European Journal* 27 (2021): 14057.

15. Ž. Ban, S. Griesbeck, S. Tomić, J. Nitsch, T. B. Marder, and I. Piantanida, "A Quadrupolar Bis-Triarylborane Chromophore as a Fluorimetric and Chirooptic Probe for Simultaneous and Selective Sensing of DNA, RNA and Proteins," *Chemistry – A European Journal* 26 (2020): 2195.

16. S. Griesbeck, E. Michail, C. Wang, et al., "Tuning the π-Bridge of Quadrupolar Triarylborane Chromophores for One- and Two-Photon Excited Fluorescence Imaging of Lysosomes in Live Cells," *Chemical Science* 10 (2019): 5405.

17. S. Griesbeck, M. Ferger, C. Czernetzi, et al., "Optimization of Aqueous Stability versus π-Conjugation in Tetracationic Bis(triarylborane) Chromophores: Applications in Live-Cell Imaging," *Chemistry – A European Journal* 25 (2019): 7679.

18. S. Griesbeck, Z. Zhang, M. Gutmann, et al., "Water-Soluble Triarylborane Chromophores for One- and Two-Photon Excited Fluorescence Imaging of Mitochondria in Cells," *Chemistry – A European Journal* 22 (2016): 14701.

19. D. P. Saftić, R. Ricker, P. Mentzel, et al., "Tetracationic Bis-Triarylborane Tetraynes as Dual Fluorescence and SERS Sensors for DNA, RNA and Proteins," *Microchemical Journal* 196 (2024): 109665.

20. K. Božinović, D. Nestić, C. Lambert, et al., "Diethynylarene-Linked Bis(triarylborane) cations as Theranostic Agents for Tumor Cell and Virus-Targeted Photodynamic Therapy," *Journal of Photochemistry and Photobiology B: Biology* 234 (2022): 112523.

21. M. Ferger, Ž. Ban, I. Krošl, et al., "Bis(phenylethynyl)arene Linkers in Tetracationic Bis-Triarylborane Chromophores Control Fluorimetric and Raman Sensing of Various DNA and RNA," *Chemistry – A European Journal* 27 (2021): 5142.

22. H. Amini, Ž. Ban, M. Ferger, et al., "Tetracationic Bis-Triarylborane 1,3-Butadiyne as a Combined Fluorimetric and Raman Probe for Simultaneous and Selective Sensing of Various DNA, RNA and Proteins," *Chemistry – A European Journal* 26 (2020): 6017.

23. M. M. Haley and R. R. Tykwinski, *Carbon-Rich Compounds: From Molecules to Materials* (John Wiley & Sons, 2006).

24. Z. Guo, Y. Wang, J. Heitmüller, et al., "Ultrafast Photophysics of *para*-Substituted 2,5-Bis(arylethynyl) Rhodacyclopentadienes: Thermally Activated Intersystem Crossing," *Chemical Science* 15 (2024): 14746.

25. C. Sieck, D. Sieh, M. Sapotta, et al., "Convenient Synthetic Access to Fluorescent Rhodacyclopentadienes via Ligand Exchange Reactions," *Journal of Organometallic Chemistry* 847 (2017): 184.

26. C. Sieck, M. G. Tay, M.-H. Thibault, et al., "Reductive Coupling of Diynes at Rhodium Gives Fluorescent Rhodacyclopentadienes or Phosphorescent Rhodium 2,2′-Biphenyl Complexes," *Chemistry – A European Journal* 22 (2016): 10523.

27. A. Steffen, R. M. Ward, M. G. Tay, et al., "Regiospecfic Formation and Unusual Optical Properties of 2,5-Bis(arylethynyl)rhodacyclopentadienes: A New Class of Luminescent Organometallics," *Chemistry – A European Journal* 20 (2014): 3652.

28. A. Steffen, K. Costuas, A. Boucekkine, et al., "Fluorescence in Rhoda- and Iridacyclopentadienes Neglecting the Spin-Orbit Coupling of the Heavy Atom: The Ligand Dominates," *Inorganic Chemistry* 53 (2014): 7055.

29. A. Steffen, M. G. Tay, A. S. Batsanov, et al., "2,5-Bis(*p*-Arylethynyl)-Rhodacyclopentadienes Show Intense Fluorescence: Denying the Presence of a Heavy Atom," *Angewandte Chemie International Edition* 49 (2010): 2349.

30. J. P. Rourke, A. S. Batsanov, J. A. K. Howard, and T. B. Marder, "Regiospecific High Yield Reductive Coupling of Diynes to Give a Luminescent Rhodium Complex," *Chemical Communications* (2001): 2626.

31. X. Ma, J. Maier, M. Wenzel, et al., "Direct Observation of *o*-Benzyne Formation in Photochemical Hexadehydro-Diels–Alder (*hν*-HDDA) Reactions," *Chemical Science* 11 (2020): 9198.

32. J. Maier, M. Deutsch, J. Merz, et al., "Highly Conjugated π-Systems Arising From Cannibalistic Hexadehydro-Diels-Alder Couplings: Cleavage of C-C Single and Triple Bonds," *Chemistry – A European Journal* 26 (2020): 15989.

33. L. L. Fluegel and T. R. Hoye, "Hexadehydro-Diels–Alder Reaction: Benzyne Generation via Cycloisomerization of Tethered Triynes," *Chemical Reviews* 121 (2021): 2413.

34. O. Diamond and T. B. Marder, "Methodology and Applications of the Hexadehydro-Diels-Alder (HDDA) Reaction," *Organic Chemistry Frontiers* 4 (2017): 891.

35. J. Maier and T. B. Marder, "Mechanistic and Kinetic Factors of Ortho-Benzyne Formation in Hexadehydro-Diels-Alder (HDDA) Reactions," *Chemistry – A European Journal* 27 (2021): 7978.

36. B. M. Trost and C.-J. Li, *Modern Alkyne Chemistry: Catalytic and Atom-Economic Transformations* (John Wiley & Sons, 2015).

37. B. R. Galan and T. Rovis, "Beyond Reppe: Building Substituted Arenes by [2+2+2] Cycloadditions of Alkynes," *Angewandte Chemie International Edition* 48 (2009): 2830.

38. A. Roglans, A. Pla-Quintana, and M. Solà, "Mechanistic Studies of Transition-Metal-Catalyzed [2+2+2]Cycloaddition Reactions," *Chemical Reviews* 121 (2021): 1894.

39. S. Kotha, K. Lahiri, and G. Sreevania, "Design and Synthesis of Aromatics through [2+2+2] Cyclotrimerization," *Synlett* 29 (2018): 2342.

40. K. Yamamoto, H. Nagae, H. Tsurugi, and K. Mashima, "Mechanistic Understanding of Alkyne Cyclotrimerization on Mononuclear and Dinuclear Scaffolds: [4+2] Cycloaddition of the Third Alkyne onto Metallacyclopentadienes and Dimetallacyclopentadienes," *Dalton Transactions* 45 (2016): 17072.

41. D. Broere and E. Ruijter, "Recent Advances in Transition-Metal-Catalyzed [2+2+2] Cyclo(Co)Trimerization Reactions," *Synthesis* 44 (2012): 2639.

42. G. Domínguez and J. Pérez-Castells, "Recent Advances in [2+2+2] Cycloaddition Reactions," *Chemical Society Reviews* 40 (2011): 3430.

43. T. Shibata and K. Tsuchikama, "Recent Advances in Enantioselective [2+2+2] Cycloaddition," *Organic & Biomolecular Chemistry* 6 (2008): 1317.

44. P. R. Chopade and J. Louie, "[2+2+2] Cycloaddition Reactions Catalyzed by Transition Metal Complexes," *Advanced Synthesis & Catalysis* 348 (2006): 2307.

45. S. Kotha, E. Brahmachary, and K. Lahiri, "Transition Metal Catalyzed [2+2+2] Cycloaddition and Application in Organic Synthesis," *European Journal of Organic Chemistry* 2005 (2005): 4741.

46. S. Saito and Y. Yamamoto, "Recent Advances in the Transition-Metal-Catalyzed Regioselective Approaches to Polysubstituted Benzene Derivatives," *Chemical Reviews* 100 (2000): 2901.

47. N. E. Schore, "Transition Metal-Mediated Cycloaddition Reactions of Alkynes in Organic Synthesis," *Chemical Reviews* 88 (1988): 1081.

48. R. Chakrabortty, S. Ghosh, and V. Ganesh, "Nickel-Catalyzed [2+2+2] Cyclotrimerization of Alkynes and Other Unsaturated Systems: A Literature Overview," *European Journal of Organic Chemistry* 27 (2024): e202400801.

27514765, 2026, 4, Downloaded from https://chemistry-europe.onlinelibrary.wiley.com/doi/10.1002/ceur.202500464 by Cochrane Croatia, Wiley Online Library on [24/11/2026]. See the Terms and Conditions (https://onlinelibrary.wiley.com/terms-and-conditions) on Wiley Online Library for rules of use; OA articles are governed by the applicable Creative Commons License

49. M. T. Martín, C. Maya, A. Galindo, and M. C. Nicasioa, "Ni-Catalyzed [2+2+2] Cycloaddition of Alkynes to Form Arenes and Pyridines at Low Catalyst Loadings," *Advanced Synthesis & Catalysis* 367 (2025): e202400765.

50. Y. Ma, C. Liu, D. Yang, et al., "Ligand Controlled Regio-Divergent [2+2+2] Cyclotrimerization of Alkynes by Merging Electrochemistry and Nickel Catalysis," *Advanced Synthesis & Catalysis* 00 (2025): e70075.

51. J.-C. Hsieh and C.-H. Cheng, "Nickel-Catalyzed Cocyclotrimerization of Arynes with Diynes; a Novel Method for Synthesis of Naphthalene Derivatives," *Chemical Communications* (2005): 2459.

52. Z. Li, Y. Mao, Y. Sun, et al., "Bench-Stable Nickel(II)–aryl Complex-Catalyzed Cyclotrimerisation of Diynes and Alkynes to Synthesis Multisubstituted Benzene Derivatives," *Results in Chemistry* 7 (2024): 101523.

53. For an Example of a Ni-Catalyzed 2+2+2 Cyclization Using Unlinked Buta-1,3-Diynes, see: R. Chakrabortty, S. Ghosh, and V. Ganesh, "Ni^0-Catalyzed Regioselective [2+2+2] Cyclotrimerization of 1,3- Diynes: An Expeditious Synthesis of Hexasubstituted Alkynyl Benzenes," *Organic Letters* 26 (2024): 792.

54. N. Schwenk, "*Seeing the Light: Synthesis of Luminescent Rhodacyclopentadienes and Investigations of their Optical Properties and Catalytic Activity*," (PhD Thesis, Julius-Maximilians-Universität Würzburg,Germany, 2018).

55. C. R. Cantor and P. R. Schimmel, *Biophysical Chemistry, Vol. 3*, (WH Freeman and Co., 1980).

56. M. Egli and W. Saenger, *Principles of Nucleic Acid Structure* (Springer-Verlag, 1983).

57. A. G. Doyle, J. D. Shields, E. E. Gray, and A. G. Doyle, "A Modular, Air-Stable Nickel Precatalyst," *Organic Letters* 17 (2015): 2166.

58. J. Magano and S. Monfette, "Development of an Air-Stable, Broadly Applicable Nickel Source for Nickel-Catalyzed Cross-Coupling," *ACS Catalysis* 5 (2015): 3120.

59. A. Goswami, T. Ito, and S. Okamoto, "Efficient Activation of 2-Iminomethylpyridine/Cobalt-Based Alkyne [2+2+2] Cycloaddition Catalyst by Addition of a Silver Salt," *Advanced Synthesis & Catalysis* 349 (2007): 2368.

60. L. Orian, J. N. P. Van Stralen, and F. M. Bickelhaupt, "Cyclotrimerization Reactions Catalyzed by Rhodium(I) Half-Sandwich Complexes: A Mechanistic Density Functional Study," *Organometallics* 26 (2007): 3816.

61. J. A. Varela and C. Saá, "CpRuCl- and CpCo-Catalyzed or Mediated Cyclotrimerizations of Alkynes and [2+2+2] Cycloadditions of Alkynes to Alkenes: A Comparative DFT Study," *Journal of Organometallic Chemistry* 694 (2009): 143.

62. A. Dachs, A. Torrent, A. Pla-Quintana, A. Roglans, and A. Jutand, "Rates and Mechanism of Rhodium-Catalyzed [2+2+2] Cycloaddition of Bisalkynes and a Monoalkyne," *Organometallics* 28 (2009): 6036.

63. J. Sauer, "Diels-Alder Reactions II: The Reaction Mechanism," *Angewandte Chemie International Edition in English* 6 (1967): 16.

64. G. K. Kole, M. Košćak, A. Amar, et al., "Methyl Viologens of Bis-(4′-Pyridylethynyl)arenes - Structures, Photophysical and Electrochemical Studies, and Their Potential Application in Biology," *Chemistry – A European Journal* 28 (2022): e202200753.

65. G. K. Kole, J. Merz, A. Amar, et al., "2- and 2,7-Substituted para-N-Methylpyridinium Pyrenes: Syntheses, Molecular and Electronic Structures, Photophysical, Electrochemical, and Spectroelectrochemical Properties and Binding to Double Stranded (ds)-DNA," *Chemistry – A European Journal* 27 (2021): 2837.

66. S. J. Greaves, E. L. Flynn, E. L. Futcher, et al., "Cavity Ring-Down Spectroscopy of the Torsional Motions of 1,4-Bis(phenylethynyl)benzene," *Journal of Physical Chemistry A* 110 (2006): 2114–2121.

67. L. Giordano, V. V. Shvadchak, J. A. Fauerbach, E. A. Jares-Erijman, and T. M. Jovin, "Highly Solvatochromic 7-Aryl-3-Hydroxychromones," *Journal of Physical Chemistry Letters* 3 (2012): 1011.

68. J. Do, J. Huh, and E. Kim, "Solvatochromic Fluorescence of Piperazine-Modified Bipyridazines for an Organic Solvent-Sensitive Film," *Langmuir* 25 (2009): 9405.

69. C. Zhou, D. Cong, Y. Gao, et al., "Enhancing the Electroluminescent Efficiency of Acridine-Based Donor–Acceptor Materials: Quasi-Equivalent Hybridized Local and Charge-Transfer State," *Journal of Physical Chemistry Letters* 122 (2018): 18376.

70. H. Van Mullekom, J. Vekemans, E. Havinga, and E. Meijer, "Developments in the Chemistry and Band Gap Engineering of Donor–acceptor Substituted Conjugated Polymers," *Materials Science and Engineering: R: Reports* 32 (2001): 1.

71. R. Englman and J. Jortner, "The Energy Gap Law for Radiationless Transitions in Large Molecules," *Molecular Physics* 18 (1970): 145.

72. D. Lin-Vien, N. Colthup, W. Fateley, and J. Grasselli, *The Handbook of Infrared and Raman Characteristic Frequencies of Organic Molecules. Chapter 8: The –C≡N and –N≡C Groups* (Academic Press, 1991).

73. J. D. McGhee and P. H. von Hippel, "Theoretical Aspects of DNA-Protein Interactions: Co-Operative and Non-Co-Operative Binding of Large Ligands to a One-Dimensional Homogeneous Lattice," *Journal of Molecular Biology* 86 (1974): 469.

74. G. Scatchard, "The Attractions of Proteins for Small Molecules and Ions," *Annals of the New York Academy of Sciences* 51 (1949): 660.

75. M. G. Gore, *Spectrophotometry and Spectrofluorimetry. A Practical Approach* (Oxford University Press, 2000).

76. L. M. Tumir, I. Piantanida, I. Juranović, Z. Meić, S. Tomić, and M. Žinić, "Recognition of Homo-Polynucleotides Containing Adenine by a Phenanthridinium Bis-Uracil Conjugate in Aqueous Media," *Chemical Communications* (2005): 2561.

77. A. C. Sedgwick, J. T. Brewster, T. H. Wu, et al., "Indicator Displacement Assays (IDAs): The Past, Present and Future," *Chemical Society Reviews* 50 (2021): 9.

78. R. Palchaudhuri and P. U. Hergenrother, "DNA as a Target for Anticancer Compounds: Methods to Determine the Mode of Binding and the Mechanism of Action," *Current Opinion in Biotechnology* 18 (2007): 497.

79. W. C. Tse and D. L. Boger, "A Fluorescent Intercalator Displacement Assay for Establishing DNA Binding Selectivity and Affinity," *Accounts of Chemical Research* 37 (2004): 61.

80. A. Rodger and B. Norden, *Circular Dichroism and Linear Dichroism* (Oxford University Press, 1997).

81. T. Šmidlehner, I. Piantanida, and G. Pescitelli, "Polarization Spectroscopy Methods in the Determination of Interactions of Small Molecules with Nucleic Acids - Tutorial," *Beilstein Journal of Organic Chemistry* 14 (2018): 84.

82. M. Eriksson and B. Norden, "Linear and Circular Dichroism of Drug-Nucleic Acid Complexes," *Methods in Enzymology* 340 (2001): 68.

83. N. H. List, J. Knoops, J. Rubio-Magnieto, et al., "Origin of DNA-Induced Circular Dichroism in a Minor-Groove Binder," *Journal of the American Chemical Society* 139 (2017): 14947.

84. W. B. Hu, C. Blecking, M. Kralj, L. Suman, I. Piantanida, and T. Schrader, "DNA Recognition with Polycyclic-Aromatic-Hydrocarbon-Presenting Calixarene Conjugates," *Chemistry – A European Journal* 18 (2012): 3589.

85. L. A. Reis and M. S. Rocha, "DNA Interaction with DAPI Fluorescent Dye: Force Spectroscopy Decouples Two Different Binding Modes," *Biopolymers* 107 (2017): e23015.

86. J. L. Mergny and L. Lacroix, "Analysis of Thermal Melting Curves," *Oligonucleotides* 13 (2003): 515.

27514765, 2026, 4, Downloaded from https://chemistry-europe.onlinelibrary.wiley.com/doi/10.1002/ceur.202500464 by Cochrane Croatia, Wiley Online Library on [24/11/2026]. See the Terms and Conditions (https://onlinelibrary.wiley.com/terms-and-conditions) on Wiley Online Library for rules of use; OA articles are governed by the applicable Creative Commons License

87. I. Jarak, M. Marjanović, I. Piantanida, M. Kralj, and G. Karminski-Zamola, "Novel Pentamidine Derivatives: Synthesis, Anti-Tumor Properties and Polynucleotide-Binding Activities," *European Journal of Medicinal Chemistry* 46 (2011): 2807.

88. M. Demeunynck, C. Bailly, and W. D. Wilson, *Small Molecule DNA and RNA Binders: From Synthesis to Nucleic Acid Complexes*, (Wiley-VCH Verlag GmbH & Co, KGaA, 2004).

89. A. E. Brown and B. E. Eichler, "Symmetric Diarylacetylenes: One-Pot Syntheses and Solution Photoluminescence," *Tetrahedron Letters* 52 (2011): 1960.

90. P. T. Nguyen, H. T. Nguyen, H. Q. Pham, J. Kim, K. E. Cordova, and H. Furukawa, "Synthesis and Selective CO_2 Capture Properties of a Series of Hexatopic Linker-Based Metal–Organic Frameworks," *Inorganic Chemistry* 54 (2015): 10065.

91. J. Zhang and T. R. Hoye, "Divergent Reactivity during the Trapping of Benzynes by Glycidol Analogs: Ring Cleavage via Pinacol-Like Rearrangements vs Oxirane Fragmentations," *Organic Letters* 21 (2019): 2615.

92. Z. Zhou, J. Yu, J. F. Colell, et al., "Long-Lived $^{13}C_2$ Nuclear Spin States Hyperpolarized by Parahydrogen in Reversible Exchange at Microtesla Fields," *Journal of Physical Chemistry Letters* 8 (2017): 3008.

93. A. Vogt, *Aufbau Neuer, Funktionaler Chromophore Aus Acetylenen*, (ETH Zurich 2009).

94. Y. Yamaguchi, T. Ochi, Y. Matsubara, and Z.-i. Yoshida, "Highly Emissive Whole Rainbow Fluorophores Consisting of 1,4-Bis(2-Phenylethynyl) Benzene Core Skeleton: Design, Synthesis, and Light-Emitting Characteristics," *Journal of Physical Chemistry A* 119 (2015): 8630.

95. J. Tydlitát, M. Fecková, P. Le Poul, et al., "Influence of Donor-Substituents on Triphenylamine Chromophores Bearing Pyridine Fragments," *European Journal of Organic Chemistry* 2019 (2019): 1921.

96. G. M. Sheldrick, "SHELXT - Integrated Space-Group and Crystal-Structure Determination," *Acta Crystallographica Section A: Foundations and Advances* 71 (2015): 3.

97. G. M. Sheldrick, "A Short History of SHELX," *Acta Crystallographica Section A: Foundations of Crystallography* 64 (2008): 112.

98. C. B. Hübschle, G. M. Sheldrick, and B. Dittrich, "ShelXle: A Qt Graphical User Interface for SHELXL," *Journal of Applied Crystallography* 44 (2011): 1281.

99. J. Gershberg, M. Radić Stojković, M. Škugor, et al., "Sensing of Double-Stranded DNA/RNA Secondary Structures by Water Soluble Homochiral Perylene Bisimide Dyes," *Chemistry – A European Journal* 21 (2015): 7886.

100. T. Mosmann, "Rapid Colorimetric Assay for Cellular Growth and Survival: Application to Proliferation and Cytotoxicity Assays," *Journal of Immunological Methods* 65 (1983): 55.

Supporting Information

Additional supporting information can be found online in the Supporting Information section. All synthetic procedures and compound characterization, X-ray crystallographic data, structural properties of DNA's and RNA's studied, physico-chemical properties of the compounds studied in aqueous solutions, additional experimental data (fluorimetric and CD titrations, thermal denaturation experiments) of interactions with biomacromolecules. The authors have cited additional references within the Supporting Information [89–100].

27514765, 2026, 4, Downloaded from https://chemistry-europe.onlinelibrary.wiley.com/doi/10.1002/ceur.202500464 by Cochrane Croatia, Wiley Online Library on [24/11/2026]. See the Terms and Conditions (https://onlinelibrary.wiley.com/terms-and-conditions) on Wiley Online Library for rules of use; OA articles are governed by the applicable Creative Commons License